Universiteit Utrecht

Opleiding Natuur- en Sterrenkunde

The nonlinear response of a Helmholtz oscillator in an interacting, double tidal inlet system

Bachelor Thesis

Lars Verboven

Supervisors:

Prof Dr. H.E. de Swart
Institute for Marine and Atmospheric research Utrecht

Prof. Dr. L.R.M. Maas
Institute for Marine and Atmospheric research Utrecht

28 July 2021

Image: top view of Ilha da Culatra, Portugal. This island creates two inlets in the bay of Faro. Source: http://www.lugaraosul.pt/.

Abstract

Certain field observations indicate irregular tidal oscillations within almost enclosed coastal basins connected to the sea through a narrow channel. Previous studies have explained this using models of Helmholtz resonators which incorporate sloping basin bottoms. These sloping bottoms trigger a nonlinear volume response to external tides coming from the sea. These studies suggest that the nonlinear response of a sloping basin bottom is more pronounced when the basin is near Helmholtz resonance, leading to tides having multiple dynamical equilibria or even exhibit chaotic behaviour within the basin.

However, situations where the almost enclosed basin is connected to the sea through multiple channels has not gotten as much exposure in research. This leads, in general, to multiple coupled oscillator equations.

This thesis aims to extend the model of the aforementioned articles to a system with two connecting channels and where the coastal basin is, due to a natural barrier, split into two sub-basins that are allowed to interact with each other. It is researched whether similar or new nonlinear effects arise in the extended model.

The results imply that the nonlinearities in the extended model still causes, when near Helmholtz resonance, multiple equilibria and chaotic behaviour. In addition, the results suggest that multiple equilibria and chaotic effects may even occur for some basins only if they interact which each other, and not when seperated from each other.

Contents

1 Introduction

Many coastal embayments worldwide are connected to the sea in the form of a *tidal inlet system*. This consists of a coastal basin which is almost enclosed, called the backbarrier basin, that is connected to the sea only by way of one or multiple narrow channels, called inlets. Notable examples of tidal inlet systems are the Dutch Wadden Sea, or the bay of Faro. An external tide is then able to flow through these inlets into the coastal basin, causing the interior water of the basin to experience tidal motion.
The role of external tide arriving in tidal inlet systems is played by ocean tides. Conventional wisdom suggests that these tides behave very regularly. Yet, within certain tidal inlet systems, there actually exist reports on *irregular* tides. An example is [1] which reported irregularities in tide observations in Moldefjord, Norway that suggest chaotic tidal behaviour. In fact, such reports on irregular tides have already started to appear as early as 1908 (see [2] and references therein). Given the regularity for which tides seem to be known, the notion of chaotic tides is remarkable.
If tides within tidal inlet systems would indeed be chaotic, it would have serious implications on the corresponding ecosystems. For example, the net transport of sediment is determined by tides; disruptive transport of sediment might result in a sediment imbalance in tidal inlet systems, which can be detrimental for the health of the ecosystem ([3]). In addition, fishermen or sailors, for example, could be hindered if the usual timing of ebb and flood in coastal bays would become different, or in fact, unpredictable (i.e. chaotic).
Previous research ([4] and [2], hereafter referred to as 'M97' and 'MD' respectively) have used models of a Helmholtz oscillator to explain these irregular effects. In particular, these studies included a realistic description of the hypsometry of the basin in their model, i.e. a linearly sloping basin bottom. Linearly sloping bottoms give the Helmholtz oscillator a nonlinear restoring mechanism, which leads to a nonlinear differential equation describing the tides within the system (see M97 for a detailed discussion).
An important role in these studies is also played by Helmholtz resonance. This resonance is possible because tidal inlet systems possess a certain eigenfrequency, called the Helmholtz frequency, which is determined by their geometric dimensions. When the external tide arriving at the tidal inlet system has a frequency close to the Helmholtz frequency, the tides in the basin will experience a resonant response, strongly boosting its amplitude ([5]).
These studies suggest that the nonlinear response of the basin due to its hypsometry is more pronounced when in Helmholtz resonance; the nonlinear response then triggers the occurrence multiple steady states, when the external tide was modeled as a sinusoid, and even chaotic behaviour, when the external tide was modeled as a quasi-periodic tide.
In this thesis, the models used in M97 and MD is extended to a situation where there are two tidal inlet systems neighbouring each other, of which the basins are separated by a water shed[1]. This is also referred to below as a 'double tidal inlet system', and a system with one basin and one inlet is referred to as 'a single tidal inlet system'. Through the water shed the two basins are allowed to exchange a limited amount of volume and therefore 'interact' with each other. Since many tidal inlet systems in the world have multiple inlets and contain water shed structures, it is useful to consider such a model. The Dutch Wadden Sea is an

[1]Note that such a system can also be interpreted as one large basin with two inlets instead of one, where the basin is divided into two parts by a water shed lying between the two inlets.

example of such a system. The inclusion of interaction via a water shed could possibly change the effect of Helmholtz resonance, which could amplify, modify or reduce the occurrence of the tidal irregularities found in M97 and MD.
The research question of this thesis is as follows: *What are the effects of allowing interaction between two nonlinear, single tidal inlet systems?*
Relevant sub-questions include:
(1) How do the tides in the two basins behave, for two special bottom descriptions, i.e. vertical sidewalls and linearly sloping sidewalls, when they interact with each other?
(2) Does interaction between two basins change the effect of Helmholtz resonance in those basins?
(3) Are the nonlinear effects seen in M97 and MD still possible in an interacting, double tidal inlet system?
(4) Do new nonlinear effects appear when interaction between the basins is allowed?
This thesis is structured as follows. In chapter 2, the model used for the double tidal inlet system is explained in detail and a derivation of the coupled differential equations describing this model is given. These equations are analytically solved in chapter 3 for a vertical sidewall bottom description, for which the differential equations are linear. This model is then further refined by taking the bottom description used by M97 and MD, for which the corresponding nonlinear differential equations are discussed; a design of the numerical simulations needed to analyse these equations is given. In chapter 4, the analysis of aforementioned analytical solutions is presented, as well as the results of the numerical simulations for the nonlinear model. The results are discussed in chapter 5 and an outlook for further research is given. Chapter 6 concludes with a summary of the answers to the research question and the sub-questions.

2 Theoretical setup

2.1 Physical setting and assumptions

To analyse the behaviour of a double tidal inlet system, we introduce a mathematical model as a stylized version of such a system. This section aims to illustrate the model used in calculations in later sections. Figure 1 sketches the situation at hand.

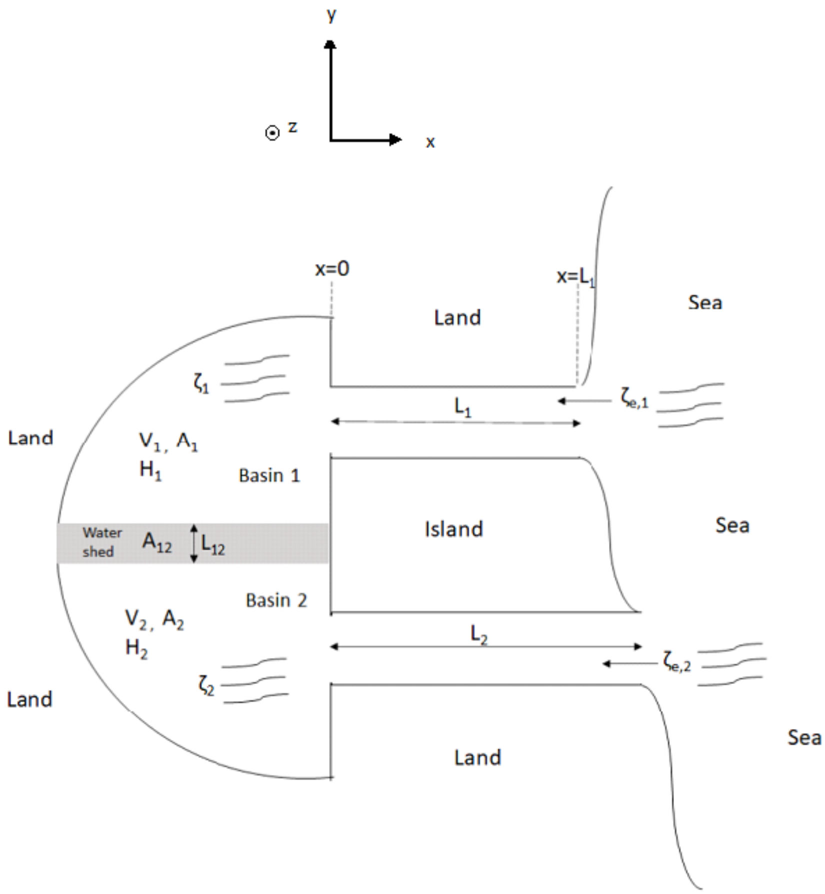

Figure 1: A double, interacting tidal inlet system. The channels have lengths L_1 and L_2 respectively. The sea provides an external tide, given by $\zeta_{e,1}$ for basin 1 and $\zeta_{e,2}$ for basin 2, which forces currents to move through the channels to the basin entrances. The basin entrances are, in this picture, both located at $x = 0$. The water surface levels within basin 1 and 2 are denoted by ζ_1 and ζ_2 respectively, A_i denotes the horizontal wetted area of basin i and H_i denotes the maximum depth of basin i, measured from mean water level downwards. V_i denotes the excess volume contained basin i, that is: the total amount of volume present minus the time-averaged mean volume of the basin, i.e. a net volume. The interaction area provided by the water shed is indicated with grey coloring, and has length L_{12} and vertical cross-sectional area A_{12}.

In Figure 1, it is illustrated how the sea borders the right-hand exit of the channels and

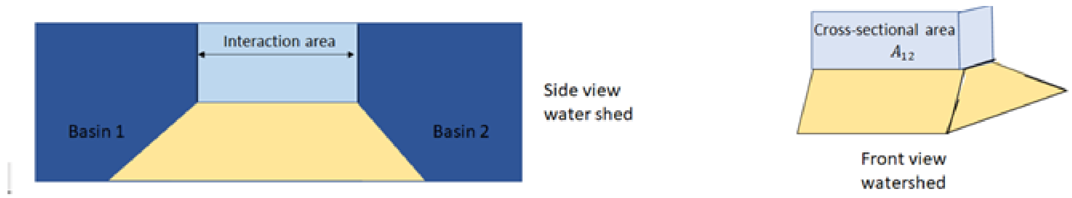

Figure 2: Left: schematic side view of the water shed. The water shed is indicated with a lighter blue colour, because it is more shallow than the basins. Right: oblique view of the same water shed, indicating its cross-secetional area A_{12}.

mainland borders the left-hand boundary of the backbarrier basin. The two inlets are created by narrow gaps between a coastal island (in the middle) and the mainland (top and bottom respectively). The axis layout is also included at the top. We also note that $z = 0$ is chosen such that it coincides with the mean[2] water level of basin 1 (this is not visible in Figure 1). The water surface elevation profile within basin i is denoted by $\zeta_i = \zeta_i(x, y, t)$ and the external tide arriving at the inlet to basin i is denoted by $\zeta_{e,i}$.
A convenient way of keeping track of the volumes of the basins during mass-exchange is to use the variable *excess volume* instead of regular volume. The excess volume $V_i(t)$ of basin i is defined as the total volume present at time t minus the time-averaged mean volume. In contrast to regular volume, the excess volume can also become negative. The convenience is that one can immediately tell from the sign of V_i at what stage of the oscillation basin i is, i.e. either it has obtained mass from the sea or it has given some mass to the sea.
The basins and inlets have some important geometric characteristics: basin i possesses mean horizontal wetted basin area $A_{0,i}$, where the subscript 0 denotes the mean with respect to the z-coordinate. This area can be understood as the horizontal wetted area at mean water level $z = 0$ when external tides are absent. The maximum depth of the basins is given by H_i, which is assumed to also be the depth of inlet i. This means that basin i and the inlet leading to it have the same characteristic vertical scale. Furthermore, the inlet of basin i has length L_i and a vertical cross-sectional wetted area $A_{c,i}$, where subscript 'c' denotes 'cross-sectional'.
Between the two basins there is a so-called water shed, which functions as a transition area and provides an opportunity for interaction between the two basins[3]. A water shed exists by virtue of a wall-like structure between two parts of the total backbarrier basin (this creates the two parts basin 1 and basin 2) which is a lot more shallow than the other parts of the backbarrier basin. An illustration of a water shed is given in Figure 2. The water shed area is indicated by the yellow part and is, as illustrated, assumed to also be submerged under the water level. As such, the water shed possesses a vertical cross-sectional wetted area A_{12} and a length L_{12} in the y-direction, see also Figure 1. In section 2.2 below, it will be argued that the water shed provides dynamical interaction between the water levels of basin 1 and basin 2.
Before proceeding to the derivation of equations of motion, there are some simplifying assumptions. These are the following:

[2]That is, mean with respect to time.

[3]The name 'water shed' refers to a situation where the water level falls and the wall-like structure between the two basins is *not* completely submerged anymore; the structure would then *shed* the water to basin 1 on one side and to basin 2 on the other side.

1) The length dimensions in the x-direction of the basins are very small compared to the wavelengths of the external tides. This has the effect that the external waves arriving at a basin's entrance will traverse the respective basin instantly. The water level of basin i therefore rises at every point in the basin simultaneously and also falls everywhere simultaneously, i.e. $\zeta_i(x, y, t) = \zeta_i(t)$. This implies that there are no horizontal variations of the tide within basin i, which allows us to describe the system by the global variable excess volume V_i.

2) The surface elevation is assumed to drop linearly over the length of the inlet and is taken to be very small compared the maximum depth of basin i: $\zeta_{s,i} \ll H_i$, where $\zeta_{s,i}$ is the surface elevation in inlet i. Because of this, the total vertical cross-sectional area $A_{c,i} = W_i(H_i + \zeta_{s,i})$ can be approximated as $A_{c,i} = W_i H_i$.

3) The vertical cross-sectional area $A_{c,i}$ of channel i is assumed to be spatially uniform along inlet i; this corresponds to uniform depth H_i along strait i and uniform width W_i (we model the inlets as rectangles). In a similar fashion, the vertical cross-sectional area A_{12} is assumed to be constant.

4) The inlets are narrow: $W_i \ll L_i$ where W_i is the width and L_i is the length of inlet i. This effectively makes the flow velocity within the channels fully in the downstream (along the x-axis).

5) The bottom of the watershed is assumed to be a horizontal plane, as depicted in the side view in figure 4.

As mentioned in the introduction, this thesis will focus on Helmholtz oscillation in describing the dynamics of the tidal inlet system. A Helmholtz oscillator is a system where an almost enclosed container is connected to its environment only through a narrow gap which triggers a periodic exchange between fluid in the container and fluid of the outside through the narrow opening. An example of such a system is an opened, empty bottle. In particular, due to the configuration of a narrow opening and a wider container, a natural frequency scale arises, which is called the Helmholtz frequency. This is an eigenfrequency of the oscillation, which is determined by the geometric dimensions of the container and the narrow opening.
In a tidal inlet system, the role of the container is played by the backbarrier basin and the narrow opening is represented by the narrow inlet. The fluids that are periodically exchanged are the water within the basin and the water in the sea. This exchange is brought about by a pressure difference between the basin entrance and the sea entrance. Furthermore, the Helmholtz frequency is now given by the geometric dimensions of the basin and the inlet. Resonance then occurs when the external tide has a frequency close to the Helmholtz frequency. As a consequence, the tide within the basin will then be significantly amplified. See [5] for a detailed discussion.
We note, however, that the behaviour of a tidal inlet system in general is determined by multiple modes. Aside from the mode which is described by a Helmholtz oscillator, called the Helmholtz mode, there are also the so-called sloshing modes. These are the modes that would already be present if the backbarrier basin were completely enclosed. When they are

connected to the sea via a narrow inlet, the Helmholtz mode is added to the system. Despite the presence of the other modes, we focus on the Helmholtz mode in this thesis. This is because, in short[4] basins, this mode is energetically dominant over the other modes ([6]).

2.2 Equations of motion and boundary conditions

We now seek a mathematical description of the Helmholtz mode, which is prevalent in basins that are short in the sense of assumption 1). As mentioned in assumption 1 in section 2.1, we can then use the excess volumes V_1, V_2 to describe the dynamics of the two tidal inlet systems. In appendix A.1, the following expressions are derived for V_1, V_2:

$$\frac{dV_1}{dt} = -A_{c,1}u_1 - A_{12}u_{12}, \tag{1}$$

$$\frac{dV_2}{dt} = -A_{c,2}u_2 + A_{12}u_{12}, \tag{2}$$

where:

V_i is the excess volume of basin i, which is given by $V_i = \int_0^{\zeta_i} A_i(z)\, dz$, where

$A_i(z)$ is the horizontal wetted area at height z,

ζ_i is the surface elevation in basin i

$A_{c,i}$ is the cross sectional area of the inlet channel leading to basin i;

A_{12} is the wetted vertical cross-sectional area of the water shed;

u_i is the depth-averaged flow velocity of water flowing into basin i, given by $u_i = \frac{\int_{-H_i}^{\zeta_i} \widetilde{u}_i dz}{\int_{-H_i}^{\zeta_i} dz}$;

$\widetilde{u}_i$ is the true flow velocity of water flowing into basin i;

u_{12} is the depth-averaged flow velocity of water flowing through the interaction area, calculated from the true flow analogously to u_1.

Expressions for the variables u_1, u_2 and u_{12} are also derived in the appendix:

$$\frac{du_1}{dt} = \frac{g}{L_1}(\zeta_1 - \zeta_{e,1}) - \frac{\hat{c}_1}{H_1}u_1, \tag{3}$$

$$\frac{du_2}{dt} = \frac{g}{L_2}(\zeta_2 - \zeta_{e,2}) - \frac{\hat{c}_2}{H_2}u_2, \tag{4}$$

$$0 = \frac{g}{L_{12}}(\zeta_1 - \zeta_2) - \frac{\hat{c}_{12}}{H_{12}}u_{12}, \tag{5}$$

[4] In assumption 1) of section 2.1 it was stipulated that we consider short basins.

where:

$\zeta_{e,i}$ is the external tide arriving at inlet i.

g is the acceleration of gravity;

L_i is the length of inlet i;

L_{12} is the length of the interaction area;

H_i is the depth of basin i;

H_{12} is the depth of the interaction area;

$\hat{c}_i$ is a linearized bottom friction coefficient belonging to basin i;

$\hat{c}_{12}$ is the linearized bottom friction belonging to the water shed.

Equations (1) and (2) represent conservation of mass in basin 1 and 2 respectively; the different terms on the right in equations (1) and (2) represent sources of water that may flow into the basin during time interval dt. The equations for u_1, u_2 and u_{12} represent a change in flow velocity due to a pressure difference (first term on the right in equation (3), (4) and (5)) arising from a difference in surface elevation. The second terms on the right-hand sides of equations (3), (4) and (5) respectively are linear bottom friction terms.
Note that the bottom friction coefficients carry an inverse dependence on bottom depth. This ensures that the friction becomes infinite when the water flow is along the bottom of the basin[5]. This is particularly significant for equation (5), describing the interaction in the water shed: if $H_{12} = 0$, we see, by rewriting $u_{12} = \frac{H_{12}}{\hat{c}_{12}} \frac{g}{L_{12}} (\zeta_1 - \zeta_2)$, that $u_{12} = 0$, i.e. there is no flow from basin 1 to 2 and therefore no interaction.
In appendix B, equations (1)-(5) are nondimensionalized using characteristic scales belonging to tidal inlet system 1: $V_i = A_{0,1} H_1 V_i'$, $z = H_1 z'$, $A_i(z/H_1) = A_{0,1} A_i'(z')$, $\zeta_i = H_1 \zeta_i'$, $\zeta_{e,i} = H_1 \zeta_{e,i}'$, $u_i = \frac{g H_1}{L_1 \sigma_{H,1}} u_i'$, $u_{12} = \frac{g H_1}{L_1 \sigma_{H,1}} u_{12}'$, $t = \frac{t'}{\sigma_{H,1}}$, for $i = 1, 2$, where $\sigma_{H,1}$ is the Helmholtz frequency of basin 1, which is defined as

$$\sigma_{H,1} = \sqrt{\frac{g A_{c,1}}{A_{0,1} L_1}}. \tag{6}$$

The new, scaled equations read

$$\frac{du_1}{dt} = \zeta_1 - \zeta_{e,1} - \frac{c_1}{H_1} u_1, \tag{7}$$

$$\frac{du_2}{dt} = \frac{L_1}{L_2}(\zeta_2 - \zeta_{e,2}) - \frac{c_2}{H_2} u_2, \tag{8}$$

[5]When the maximum depth H_i is zero, the bottom is located at mean water level $z = 0$, where the depth-averaged flow u_i is defined to flow.

$$\frac{dV_1}{dt} = -u_1 - A_{12,r}u_{12}, \tag{9}$$

$$\frac{dV_2}{dt} = -\frac{A_{c,2}}{A_{c,1}}u_2 + A_{12,r}u_{12}, \tag{10}$$

$$0 = \zeta_1 - \zeta_2 - \frac{c_{12}}{H_{12}}u_{12}, \tag{11}$$

where we renamed $\frac{c_i}{H_i} = \frac{1}{\sigma_{H,1}}\frac{\hat{c}_i}{H_i}$, $\frac{c_{12}}{H_{12}} = \frac{L_{12}}{gH_1}\frac{\hat{c}_{12}}{H_{12}}$ and $A_{12,r} = \frac{A_{12}}{A_{c,1}}$. Furthermore, note that $\frac{A_{c,2}}{A_{c,1}}\frac{L_1}{L_2} = \left(\frac{\sigma_{H,2}}{\sigma_{H,1}}\right)^2 A_{2,r}$, where $A_{2,r} \equiv \frac{A_{0,2}}{A_{0,1}}$. With these expressions in mind, equations (7)-(11) are decoupled to arrive at the following coupled Helmholtz oscillator equations in terms of only V_1 and V_2:

$$\begin{aligned} \frac{d^2V_1}{dt^2} + \zeta_1(V_1) = \zeta_{e,1}(t) &- \frac{H_{12}}{c_{12}}A_{12,r}\left(\frac{\partial\zeta_1}{\partial V_1}\frac{dV_1}{dt} - \frac{\partial\zeta_2}{\partial V_2}\frac{dV_2}{dt}\right) \\ &- \frac{c_1}{H_1}\frac{H_{12}}{c_{12}}A_{12,r}\left[\zeta_1(V_1) - \zeta_2(V_2)\right] - \frac{c_1}{H_1}\frac{dV_1}{dt}, \end{aligned} \tag{12}$$

$$\begin{aligned} \frac{d^2V_2}{dt^2} + \left(\frac{\sigma_{H,2}}{\sigma_{H,1}}\right)^2 A_{2,r}\zeta_2(V_2) = \left(\frac{\sigma_{H,2}}{\sigma_{H,1}}\right)^2 &A_{2,r}\zeta_{e,2}(t) \\ &+ \frac{H_{12}}{c_{12}}A_{12,r}\left(\frac{\partial\zeta_1}{\partial V_1}\frac{dV_1}{dt} - \frac{\partial\zeta_2}{\partial V_2}\frac{dV_2}{dt}\right) \\ &+ \frac{c_2}{H_2}\frac{H_{12}}{c_{12}}A_{12,r}\left[\zeta_1(V_1) - \zeta_2(V_2)\right] - \frac{c_2}{H_2}\frac{dV_2}{dt}, \end{aligned} \tag{13}$$

where we note that ζ_i is a function of V_i through inversion of $V_i = \int_0^{\zeta_i} A_i(z)\,dz$ and that the chain rule was used: $\frac{d\zeta_i}{dt} = \frac{\partial\zeta_i}{\partial V_i}\frac{dV_i}{dt}$.

Equations (12) and (13) describe Helmholtz oscillation for excess volumes V_1, V_2 in an interacting, double tidal inlet system. Note that the precise form of equations (12) and (13) for V_1 and V_2 depends on the expression for the terms $\zeta_1(V_1), \zeta_2(V_2)$ respectively. It will be discussed in section 3 that the form of $\zeta_i(V_i)$ wholly depends on the shape of the bottom of the basin. Moreover, as explained in Appendix A, the terms $\zeta_1(V_1)$ and $\zeta_2(V_2)$ represent restoring terms. Therefore, the restoring process in equations (12) and (13) will be different for different basin shapes. This will be further discussed in the next section.

3 Methods

In this section, two kinds of sidewall configurations for the basins are explored, as well as the methods used to analyse these systems.
Firstly, the scenario where the sidewalls are vertical is studied. Although vertical sidewalls approximate coastlines rather crudely, this simpler case will be useful throughout this thesis. Vertical sidewalls gives rise to linear differential equations for the excess volumes of the basins. For this system, analytical methods are shown that produce explicit solutions $V_1(t), V_2(t)$ to equations (12) and (13).
Secondly, the scenario where the sidewalls are linearly sloping is considered. This yields nonlinear differential equations for the volumes; the numerical methods to study these are explained, including a design of performed numerical experiments.

3.1 Vertical sidewalls: linear Helmholtz oscillator

The goal of this subsection is to analyse the double tidal inlet system with vertical sidewalls. It will become clear below that such a sidewall configuration results in a linear differential equation for excess volumes V_1 and V_2.
When the basins have vertical sidewalls, the basins have a rectangular shape, as on the left in Figure 3. Therefore, the wetted horizontal cross-sectional area for basin i is constant in z and must be everywhere equal to the horizontal wetted area at mean surface level $z = 0$: $A_i(z) = A_{0,i}$. Scaled with $A_{0,1}$, we have for $i = 1, 2$:

$$A_1(z) = 1, \tag{14}$$

$$A_2(z) = \frac{A_{0,2}}{A_{0,1}} = A_{2,r}, \tag{15}$$

where $A_{2,r}$ denotes the horizontal wetted area of basin 2 relative to its counterpart in basin 1. By inverting $V_i = \int_0^{\zeta_i} A_i(z)\,dz$, expressions for ζ_1 and ζ_2 are obtained:

$$V_1 = \int_0^{\zeta_1} A_1(z)\,dz = \int_0^{\zeta_1} dz \quad \Rightarrow \quad V_1 = \zeta_1 \tag{16}$$

$$V_2 = \int_0^{\zeta_2} A_2(z)\,dz = A_{2,r} \int_0^{\zeta_2} dz \quad \Rightarrow \quad V_2 = A_{2,r}\zeta_2 \quad \Rightarrow \quad \zeta_2 = \frac{V_2}{A_{2,r}}. \tag{17}$$

Furthermore, the external tides are assumed to be pure sinusoids in time:

$$\zeta_{e,1} = Z_1 \cos(\sigma t - \varphi_1), \tag{18}$$

$$\zeta_{e,2} = Z_2 \cos(\sigma t - \varphi_2), \tag{19}$$

where σ is the frequency of the external tide, not to be confused with the Helmholtz frequency of basins 1 and 2: $\sigma_{H,1}$ and

$$\sigma_{H,2}$$

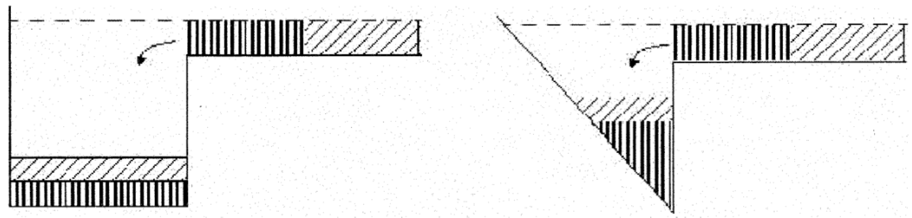

Figure 3: Source: MD. Left: a container with vertical sidewalls. Equal amounts of volume produce an equal increase of surface elevation when poured into the container, i.e. a the elevation exhibits a linear response. Right: a container with linearly sloping sidewalls. Here, equal amounts of volume produce a different increase of surface elevation when poured into the container. In particular, the increase of surface elevation depends upon how much volume is already present in the container. This points to a nonlinear response of the elevation.

. In addition, Z_i is the dimensionless amplitude of the external tide arriving at inlet i and φ_i is its phase shift. Note that σ is taken the same for $i = 1, 2$ and is scaled with Helmholtz frequency of basin 1. Taking the same σ for both inlets corresponds physically to the same tide arriving at both inlets. There can still be a phase difference ($\varphi_1 \neq \varphi_2$), because the tide needs time to propagate along the coast. We can, without loss of generality, choose the moment $t = 0$ such, that $\varphi_1 = 0$, so that only $\zeta_{e,2}$ carries a phase shift.
Using the obtained expressions for $\zeta_1, \zeta_2, \zeta_{e,1}$ and $\zeta_{e,2}$ and setting $\varphi_1 = 0$, equations (12) and (13) become

$$\begin{aligned}\frac{d^2V_1}{dt^2} + V_1 + \frac{H_{12}}{c_{12}} A_{12,r}\left(\frac{dV_1}{dt} - \frac{1}{A_{2,r}}\frac{dV_2}{dt}\right) \\ + \frac{c_1}{H_1}\frac{H_{12}}{c_{12}} A_{12,r}\left(V_1 - \frac{V_2}{A_{2,r}}\right) + \frac{c_1}{H_1}\frac{dV_1}{dt} = Z_1\cos(\sigma t),\end{aligned} \tag{20}$$

$$\begin{aligned}\frac{d^2V_2}{dt^2} + \sigma_{H,r}^2 V_2 - \frac{H_{12}}{c_{12}} A_{12,r}\left(\frac{dV_1}{dt} - \frac{1}{A_{2,r}}\frac{dV_2}{dt}\right) \\ - \frac{c_2}{H_2}\frac{H_{12}}{c_{12}} A_{12,r}\left(V_1 - \frac{1}{A_{2,r}}V_2\right) + \frac{c_2}{H_2}\frac{dV_2}{dt} = \sigma_{H,r}^2 A_{2,r} Z_2\cos(\sigma t - \varphi_2).\end{aligned} \tag{21}$$

Note that parameters Z_1 , Z_2, σ and φ_2 are characteristics of the sea/reservoir to which the basins are connected and are assumed to be external parameters that are given.
Equations (20) and (21) are, coupled, second-order linear differential equations in V_1, V_2 respectively. The linearity of these equations enables analytical solution. The equations are most easily solved by switching to matrix-vector notations.

$$\mathbf{V} = \begin{pmatrix} V_1 \\ \\ V_2 \end{pmatrix} \quad , \ \zeta_e = \begin{pmatrix} \zeta_{e,1} \\ \\ \zeta_{e,2} \end{pmatrix} \tag{22}$$

and

$$A \equiv \begin{pmatrix} \frac{c_1}{H_1} + \frac{H_{12}}{c_{12}} A_{12,r} & -\frac{H_{12}}{c_{12}}\frac{A_{12,r}}{A_{2,r}} \\ \\ -\frac{H_{12}}{c_{12}} A_{12,r} & \frac{c_2}{H_2} + \frac{H_{12}}{c_{12}}\frac{A_{12,r}}{A_{2,r}} \end{pmatrix} \tag{23}$$

$$B \equiv \begin{pmatrix} 1 + \frac{c_1}{H_1}\frac{H_{12}}{c_{12}}A_{12,r} & -\frac{c_1}{H_1}\frac{H_{12}}{c_{12}}\frac{A_{12,r}}{A_{2,r}} \\ \\ -\frac{c_2}{H_2}\frac{H_{12}}{c_{12}}A_{12,r} & \sigma^2_{H,r} + \frac{c_2}{H_2}\frac{H_{12}}{c_{12}}\frac{A_{12,r}}{A_{2,r}} \end{pmatrix}. \tag{24}$$

For brevity, in the discussion below, we will write the elements of A and B as a_{mn} and b_{mn} respectively, where $m, n = 1, 2$. Using equations (22)-(24) we recast equations (20) and (21) into matrix-vector form:

$$\ddot{\mathbf{V}} + A\dot{\mathbf{V}} + B\mathbf{V} = \zeta_e. \tag{25}$$

This is a linear inhomogeneous vector differential equation. The general solution will consist of a solution to the homogeneous equation (transient solution) and a particular solution (nontransient solution) which solves the inhomogeneous equation. For a good discussion, see [7], hereafter referred to as 'TCM'.

We will focus on the nontransient solution because of the fact that the homogeneous solutions die out in a characteristic time of $\frac{1}{c_i}$ due to the damping term $c_i\frac{dV_i}{dt}$ present in the equations for each V_i (see TCM). After that, the motion will converge to the particular solution. Since we are interested in the long term behaviour of these basins, transient solutions are not interesting.

Equation (25) is solved by writing the variables $\mathbf{V}(t)$ and $\zeta_{\mathbf{e}}(t)$ as the real parts of complex quantities $\mathbf{\Phi}(t)$ and $\mathbf{S}(t)$. Then $\mathbf{\Phi}(t)$ satisfies

$$\ddot{\mathbf{\Phi}}(t) + A\dot{\mathbf{\Phi}}(t) + B\mathbf{\Phi}(t) = \mathbf{S}(t) \tag{26}$$

Because the external tides are sinusoidal, we have

$$S_n(t) = s_n e^{i\sigma t} \quad , n = 1, 2 \tag{27}$$

where we absorbed the phases φ_n into the complex constants s_n.[6] We now make the following ansatz: $\Phi_n(t) = \phi_n e^{i\sigma t}$. Substituting equation (27) and $\mathbf{\Phi}(t) = (\phi_1, \phi_2)^T e^{i\sigma t}$ into equation (26) yields, upon dividing out $e^{i\sigma t}$ left and right:

$$\begin{pmatrix} -\sigma^2\phi_1 \\ \\ -\sigma^2\phi_2 \end{pmatrix} + A\begin{pmatrix} i\sigma\phi_1 \\ \\ i\sigma\phi_2 \end{pmatrix} + B\begin{pmatrix} \phi_1 \\ \\ \phi_2 \end{pmatrix} = \begin{pmatrix} s_1 \\ \\ s_2 \end{pmatrix}. \tag{28}$$

We see that $\mathbf{\Phi}$ satisfies the differential equation when

$$\phi_1 = \frac{s_1 - (i\sigma a_{12} + b_{12})\phi_2}{-\sigma^2 + i\sigma a_{11} + b_{11}}, \tag{29}$$

$$\phi_2 = \frac{s_2 - (i\sigma a_{21} + b_{21})\phi_1}{-\sigma^2 + i\sigma a_{22} + b_{22}}. \tag{30}$$

Note that ϕ_1 and ϕ_2 are coupled, implying a coupling of $V_1(t)$ and $V_2(t)$. Decoupling equations (29) and (30), we obtain explicit relations for ϕ_1, ϕ_2:

$$\phi_1 = \frac{(-\sigma^2 + i\sigma a_{22} + b_{22})s_1 - (i\sigma a_{12} + b_{12})s_2}{(-\sigma^2 + i\sigma a_{11} + b_{11})(-\sigma^2 + i\sigma a_{22} + b_{22}) + (i\sigma a_{12} + b_{12})(i\sigma a_{21} + b_{21})}, \tag{31}$$

[6] Index n is used here instead of i to avoid confusion with the imaginary unit i, which is present in the complex exponentials.

$$\phi_2 = \frac{(-\sigma^2 + i\sigma a_{11} + b_{11})s_2 - (i\sigma a_{21} + b_{21})s_1}{(-\sigma^2 + i\sigma a_{22} + b_{22})(-\sigma^2 + i\sigma a_{11} + b_{11}) + (i\sigma a_{21} + b_{21})(i\sigma a_{12} + b_{12})}. \tag{32}$$

Writing $\phi_n = \hat{V}_n e^{-i\delta_n}$, the solutions are

$$\mathbf{V}(t) = \begin{pmatrix} \hat{V}_1 \cos(\sigma t - \delta_1) \\ \\ \hat{V}_2 \cos(\sigma t - \delta_2) \end{pmatrix}, \tag{33}$$

where

$$V_1 = |\phi_1| \tag{34}$$

$$V_2 = |\phi_2| \tag{35}$$

$$\delta_1 = \arg(\phi_1) \tag{36}$$

$$\delta_2 = \arg(\phi_2) \tag{37}$$

The implications of these results are discussed in section 4.1. In particular, numerical plots are made to observe the how the amplitude near Helmholtz resonance ($\sigma \approx \sigma_{H,1}$) is affected by interaction strength (A_{12}), for which non-interacting tidal inlet systems are known to strongly resonate ([5]). The reason for switching to numerical calculation is due to the cumbersomeness of calculating $\hat{V}_1$, $\hat{V}_2$ from equations (31) and (32). The design of these experiments is also discussed in section 3.3.2.

We also note that a more realistic model for the external tide contains more than one frequency constituent. In fact, some tide observations have pointed out 390 different frequency constituents ([8]). Due to linearity of the vertical sidewall model, the generalization to the case of multiple frequency external tides is straightforward: the total nontransient solution will be a sum of nontransient solutions to equation (25), where, each time, ζ_e is taken equal to a different individual frequency component.

3.2 Linearly sloping sidewalls: nonlinear Helmholtz oscillator

Although the model with a rectangular-shape basin already provides a lot of information, as will be discussed in section 4.1, it still lacks a proper description of the geometry of a tidal inlet system. Coastal backbarrier basins oftentimes have a shoaling coastline as boundary instead of a vertical boundary, see again Figure 3 (right). Such shoaling coastline may be approximated mathematically as a linearly sloping basin bottom, where the horizontal wetted area for basin i at height z can be given dimensionally by the linear relation

$$A_i(z) = A_{0,i}(1 + \frac{z}{H_i}). \tag{38}$$

The offset and the slope in this expression are such that the time-mean horizontal wetted area at mean water level, $A_{0,i}$, occurs at[7] $z = 0$ and that the deepest point of basin i is

[7]As was stipulated in section 2.1, $z = 0$ is chosen to coincide with time-mean water level.

given by the maximum depth H_i: $A_i(z = -H_i) = 0$. Using the nondimensionalization $z' = z/H_1$, $A'_i(z') = A_i(z/H_1)/A_{0,1}$ (see Appendix B), we obtain

$$A'_1(z') = 1 + z', \tag{39}$$

$$A'_2(z') = \frac{A_{0,2}}{A_{0,1}}(1 + \frac{H_1}{H_2}z') \equiv A_{2,r}(1 + \frac{z'}{H_{2,r}}), \tag{40}$$

where $A_{2,r}$ is defined as in equation (15) and $H_{2,r}$ is defined as the maximum depth of basin 2 relative to that of basin 1. Dropping the primes on dimensionless variables, we determine the expressions of ζ_1, ζ_2 for these A_1, A_2:

$$V_1 = \int_0^{\zeta_1} dz\,(1 + z) = \zeta_1 + \frac{\zeta_1^2}{2}, \tag{41}$$

so that

$$\zeta_1(V_1) = \sqrt{1 + 2V_1} - 1 \tag{42}$$

where the positive square root is taken by virtue of the requirement that zero excess volume correspond to zero elevation, i.e. $V_1 = 0 \Rightarrow \zeta_1 = 0$. Analogously for basin 2, we have

$$\zeta_2(V_2) = \sqrt{H_{2,r}^2 + 2\frac{H_{2,r}}{A_{2,r}}V_2} - H_{2,r} \tag{43}$$

Now, we see from equations (42) and (43) that the restoring terms are square root in V_1, V_2 respectively, whereas in the previous section in the case of rectangular bottom, they were linear in V_1 and V_2. Also note that for small excess volumes, i.e. $V_1, V_2 \ll 1$, we have

$$\sqrt{1 + 2V_1} - 1 \simeq V_1 \tag{44}$$

$$\sqrt{H_{2,r}^2 + 2\frac{H_{2,r}}{A_{2,r}}V_2} - H_{2,r} \simeq \frac{V_2}{A_{2,r}}, \tag{45}$$

which are precisely the restoring terms of the flat bottoms in equations (16) and (17). Physically, this corresponds to the notion that small deviations of the water surface are not deep enough to 'feel' the bottom shape. This implies that the case of linearly sloping sidewalls is essentially a perturbation of the case of vertical sidewalls. This re-establishes the relevance of the previous section, where an analytical solution was produced for the vertical sidewall case. Since the evolution equation for the case of linearly sloping sidewalls reduces to that of the vertical sidewall case for small excess volumes, the solution to the former equation must reduce to the solution of the latter for small excess volumes. This means that, at moderate values of the excess volumes, one can already expect the solution for linearly sloping sidewalls to somewhat resemble the solution for vertical sidewalls.

Substituting the new equations (42) and (43) into (12) and (13) yields:

$$
\begin{aligned}
\frac{d^2V_1}{dt^2} =& \zeta_{e,1}(t) + 1 - \sqrt{1+2V_1} - \frac{c_1}{H_1}\frac{dV_1}{dt} \\
&- \frac{H_{12}}{c_{12}} A_{12,r} \left[\frac{1}{\sqrt{1+2V_1}}\frac{dV_1}{dt} - \frac{1}{\sqrt{A_{2,r}^2 + 2\frac{A_{2,r}}{H_{2,r}}V_2}}\frac{dV_2}{dt} \right] \\
&- \frac{c_1}{H_1}\frac{H_{12}}{c_{12}} A_{12,r} \left(\sqrt{1+2V_1} - \sqrt{H_{2,r}^2 + 2\frac{H_{2,r}}{A_{2,r}}V_2} + H_{2,r} - 1 \right)
\end{aligned}
\tag{46}
$$

$$
\begin{aligned}
\frac{d^2V_2}{dt^2} =& \left(\frac{\sigma_{H,2}}{\sigma_{H,1}}\right)^2 A_{2,r}\zeta_{e,2}(t) - \frac{c_2}{H_2}\frac{dV_2}{dt} \\
&- \left(\frac{\sigma_{H,2}}{\sigma_{H,1}}\right)^2 A_{2,r} \left[\sqrt{H_{2,r}^2 + 2\frac{H_{2,r}}{A_{2,r}}V_2} - H_{2,r} \right] \\
&+ \frac{H_{12}}{c_{12}} A_{12,r} \left[\frac{1}{\sqrt{1+2V_1}}\frac{dV_1}{dt} - \frac{1}{\sqrt{A_{2,r}^2 + 2\frac{A_{2,r}}{H_{2,r}}V_2}}\frac{dV_2}{dt} \right] \\
&+ \frac{c_2}{H_2}\frac{H_{12}}{c_{12}} A_{12,r} \left(\sqrt{1+2V_1} - \sqrt{H_{2,r}^2 + 2\frac{H_{2,r}}{A_{2,r}}V_2} + H_{2,r} - 1 \right).
\end{aligned}
\tag{47}
$$

Equations (46) and (47) describe the coupled Helmholtz oscillator of equations (12) and (13) when the basin bottoms slope linearly. Clearly, they contain many terms nonlinear in the excess volumes. In particular, the restoring terms $\zeta_1(V_1), \zeta_2(V_2)$ are now square root in V_1 and V_2, respectively. Unfortunately, these equations are not analytically solvable, so that we must resort numerical solution. In this thesis, a Python script utilizing Runge-Kutta 4 was employed to obtain numerical solutions.

3.3 Numerical methods

To analyse the nonlinear behaviour of two interacting tidal inlet systems with sloping bottoms, equations (46) and (47) were numerically solved for various parameter settings. In this subsection, the methodology of the plotting techniques used is first explained; after that, a design of performed experiments is given.

3.3.1 Numerical integration, Poincaré maps

An insightful way to visualize the long-term behaviour of the solutions $V_1(t), V_2(t)$ is through the use of a stroboscopic variant of phase plane plots, called the *Poincaré map*. The Poincaré map takes a phase space orbit but only shows points $(V_i, \dot{V}_i)$ evaluated at specific, regular time intervals $t = T, 2T, \ldots, nT$, where n is a positive integer and T is a chosen sampling period. Figure 4 gives an example of this. See TCM for a detailed discussion on Poincaré maps.

If the motion of a solution is strictly periodic with period T, it is easy to see that a plot

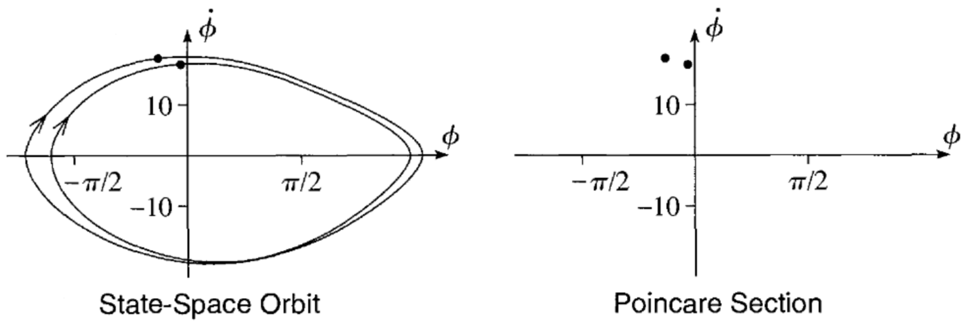

Figure 4: Two plots adapted from TCM. Left: a segment of the phase space orbit of a solution $(\phi, \dot{\phi})$ to a certain DDO equation. Right: a Poincaré map of this segment.

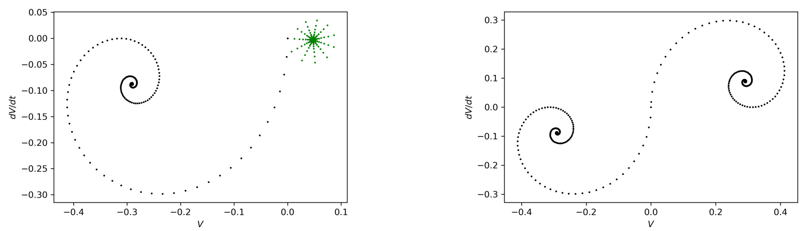

(a) (b)

Figure 5: (a) Two different Poincaré maps (black and green respectively) of some (V,$\dot{V}$) that are, at late times, periodic with the sampling period. (b) An orbit which is, at late times, periodic with twice the sampling period, thus spiraling towards two fixed points.

Poincaré map will look like a single point. Indeed, in case of T-periodicity, $(V_i(t = nT), \dot{V}_i(t = nT))$ must be the same number for every integer n.
Returning to the context of the tidal inlet system, we have from equation (33) that the nontransient solution to the (single-frequency forced) linear model is periodic with the tidal period $T = 2\pi/\sigma$. Therefore, if we choose the sampling period equal to this tidal period, the Poincaré map orbits of linearly-behaving solutions will converge toward a fixed point as transient parts of the solution fade, as in Figure 5a. It will then be easy to spot if solutions to the nonlinear equations (46) and (47) exhibit period-doubling or chaos. Any pattern in the Poincaré map that is not a spiral towards a single fixed point indicates the occurrence of some kind of nonlinear effect.
If period doubling has taken place, then it will take two tidal periods before the motion has returned to the same point $(V_i, \dot{V}_i)$. Therefore, when a Poincaré map of a period-doubled solution is sampled with the tidal period, two successive points in the Poincaré map will not be the same. Instead, every other point will be the same: $(V_i(t = nT), \dot{V}_i(t = nT)) = (V_i(t = (n+2)T), \dot{V}_i(t = (n+2)T))$. In this way the pattern in the Poincaré map will show up as two orbits each converging to their own fixed point, illustrated in Figure 5b.
For the case of quasi-periodic double frequency forcing in the linear model, the last paragraph in section 3.1 implies that the nontransient solution is also quasi-periodic. This means that at late times, the solution looks like a periodic function but is, in fact, not truly periodic. Therefore, there does not exist a sampling period T for which the Poincaré map looks like a

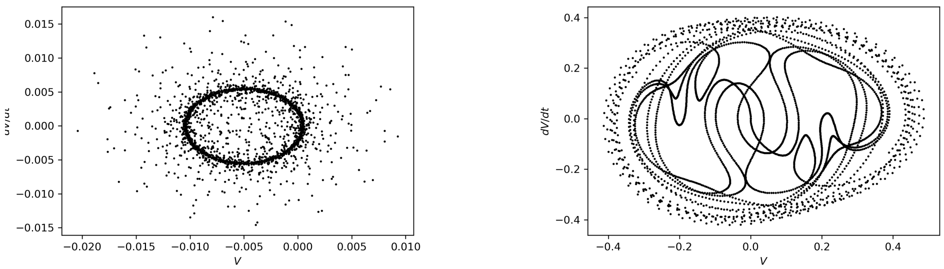

(a) (b)

Figure 6: (a) An example of some Poincaré map representing quasi-periodic motion, appearing as a closed cycle at late times (dark part of the pattern). (b) An example of some Poincaré map representing chaotic behaviour, appearing as an irregular pattern.

fixed point. Instead, because the motion never truly repeats itself, it will show up as a closed cycle of points, see Figure 6a.
In MD, it is seen that quasi-periodic double frequency forcing in the nonlinear model can lead to chaotic behaviour in some instances. Chaotic behaviour is also aperiodic behaviour, but in contrast to quasi-periodic motion, chaotic behaviour is far from periodic behaviour. Therefore, chaotic behaviour will not show up in the Poincaré map as a closed cycle but as an irregular pattern of points, see Figure 6b.
Since Poincaré maps provide an elegant way of characterizing nonlinear effects, they will be extensively used in this thesis, instead of regular phase plane orbits. In the remainder of this thesis, these four patterns in Poincaré maps are important:

1) If the Poincaré orbit tends towards one focus, no special nonlinear behaviour is present.
2) If the Poincaré orbit tends towards two foci, period doubling has taken place.
3) If the Poincaré orbit follows a closed cyclic pattern, the motion is quasi-periodic.
4) If the Poincaré orbit follows some irregular pattern at late times, the solution is chaotic.

3.4 Design of simulations

Simulations were performed in order to observe how the effect of interaction between the two basins changes earlier results for single tidal inlet systems. It is convenient to model the interaction area as a rectangular hole through a wall that separates basins 1 and 2. This wall is illustrated in Figure 7. This hole runs from basin 1 to basin 2 and its vertical cross-sectional size equals $A_{12,r}$, We can then gradually increase the strength of the interaction by increasing $A_{12,rel}$. This is visualized in Figure 8. We note that $A_{12,r} = 0$ corresponds to a hole of size zero, i.e. a solid wall fully separating both basins. Thus, when $A_{12,r} = 0$, both basins act as single tidal inlet systems. This situation will hereafter be referred to as 'no interaction'.
The friction through the rectangular hole is modeled proportional $1/\sqrt{A_{12,r}}$. Note that this prevents large volumes to be exchanged between the basins when the hole is still small, as friction proportional to $1/\sqrt{A_{12,r}}$ is large for small $A_{12,r}$.

In order to observe the effect of interaction between the basins, the experiments are performed as follows: The starting point for the simulations is $A_{12,r} = 0$, i.e. no interaction. For this the characteristic behaviour in the linear ([5]) and nonlinear models is already known from M97 and MD. Then, $A_{12,r}$ is slowly increased, corresponding to the interaction hole slowly getting bigger (see Figure 8) and we observe the effect of this on V_1 and V_2.

3.4.1 Simulations of the linear model

In order to research how the response to forcing near Helmholtz resonance ($\sigma \approx \sigma_{H,1}$) in the linear model changes when interaction is increased, numerical plots of $\hat{V}_1$ and $\hat{V}_2$ as functions of $A_{12,r}$ are made. The modeling of the interaction area is described as above (the hole). The parameters used are the following:

Table 1: Linear model

Parameter	Value
$\sigma_{H,2}/\sigma_{H,1}$	1.049
$A_{2,r}$	1
σ	varies
$A_{12,r}$	varies
c_{12}/H_{12}	$0.01/\sqrt{A_{12,r}}$
Z_1	-0.001
Z_2	-0.001
c_1/H_1	0.01
c_2/H_2	0.01
φ_1	0
φ_2	0

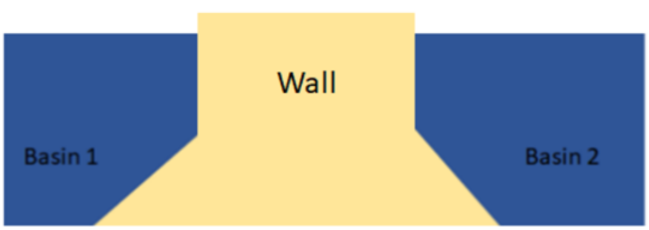

Figure 7: Schematic side view of the total backbarrier basin in the situation 'no interaction'. A wall completely separates basin 1 and 2 from each other.

Figure 8: Schematic front view of the 'wall' from Figure 7 with the hole in it, as seen face on from one of the basins. The hole is increased as $A_{12,r} = \frac{A_{12}}{A_{c,1}}$ increases.

The choice for these values is to preserve similarity to the choice made for parameters in the nonlinear model, which are explained below.

3.4.2 Experiments on the nonlinear model

As the interaction hole is increased, we use Poincaré maps for the nonlinear model to observe whether the effects seen in M97 and MD change and whether new nonlinear effects appear. This process is performed for two situations:
(i) The external tide arriving in basin i forces with one frequency, that is, $\zeta_{e,i} = Z_i \cos(\sigma t - \varphi_i)$
(ii) The external tide arriving in basin i forces quasi-periodically, that is, $\zeta_{e,i} = Z_{1,i} \cos(\sigma_1 t - \varphi_{1,i}) + Z_{2,i} \cos(\sigma_2 t - \varphi_{2,i})$, where the quotient σ_1/σ_2 is irrational.
The parameters used in the experiments are, unless otherwise indicated, as follows.
For case (i):

Table 2: Nonlinear case (i)

Parameter	Value
$\sigma_{H,2}/\sigma_{H,1}$	varies
$A_{2,r}$	varies
$A_{12,r}$	varies
c_{12}/H_{12}	$0.01/\sqrt{A_{12,r}}$
σ	2.04
Z_1	-0.1
Z_2	-0.1
c_1/H_1	0.01
c_2/H_2	0.01
φ_1	0
φ_2	0

The values of these parameters are chosen as closely as possible to figure 10b of M97, where they produce period-2 equilibria for certain initial conditions. Three comments are made regarding the parameters that are taken as variables:

- The Helmholtz resonance frequency of basin 1 is unity due to scaling; the quantity $\frac{\sigma_{H,2}}{\sigma_{H,1}}$ then allows to choose how close the Helmholtz frequency of basin 2 is to unity. Since it is argued in M97 that forcing near-resonance is a significant factor in the occurrence of period-2 steady states, we vary the variable $\frac{\sigma_{H,2}}{\sigma_{H,1}}$ across different simulations to see if forcing near-resonance plays a similar role when interaction is allowed.

- It is also indicated that $A_{12,r}$ is variable; this was already discussed in the part of section 3.4 preceding section 3.4.1.

- $A_{2,r}$ is additionally indicated as 'variable'. It should be noted that $\frac{\sigma_{H,2}}{\sigma_{H,1}} = \sqrt{\frac{L_1}{L_2}\frac{A_1}{A_2}\frac{A_{c,2}}{A_{c,1}}}$, meaning that the varying of $\frac{\sigma_{H,2}}{\sigma_{H,1}}$ and of $A_{2,r}$ are related. We make special mention of $A_{2,r}$ because it also appears in equations (46) and (47) by itself.

We remark that for these parameters, the interaction term which is the rightmost term in equations (46) and (47) is very small compared to the other interaction term (second rightmost term). Indeed, when comparing prefactors, we see that $c_1 \frac{A_{12,r}}{c_{12}} = \frac{1}{100} \cdot \frac{A_{12,r}}{c_{12}} \ll \frac{A_{12,r}}{c_{12}}$. Therefore, the smaller term is omitted in the performed simulations for simplicity.
For case (ii):

Table 3: Nonlinear case (ii)

Parameter	Value
$\sigma_{H,2}/\sigma_{H,1}$	variable
$A_{2,r}$	variable
$A_{12,r}$	variable
c_{12}/H_{12}	$0.01/\sqrt{A_{12,r}}$
σ_1	1.00
σ_2	1.01
$Z_{1,1}$	-0.001
$Z_{1,2}$	-0.001
$Z_{2,1}$	-0.001
$Z_{2,2}$	-0.001
c_1/H_1	0.001
c_2/H_2	0.001
$\varphi_{1,1}$	0
$\varphi_{1,2}$	0
$\varphi_{2,1}$	0
$\varphi_{2,2}$	0

The parameters are chosen as closely as possible to figure 11b in MD, which produce chaotic solutions for the single tidal inlet system. The same parameters are varied as in case (i). Again, the same interaction term was omitted as in case (i), for the same reason as.

4 Results

4.1 Linear model

Equation (33) suggests that pure sinusoidal forcing leads to pure sinusoidal volume oscillation. In particular, the volumes oscillate with the same frequency σ with which they are forced. However, the forcing tides and the tides within the basins are, in general, not in-phase: V_1 has phase difference $|\delta_1|$ with $\zeta_{e,1}$ and V_2 has phase difference $|\varphi_2 - \delta_2|$ with $\zeta_{e,2}$. In addition, similar to regular (uncoupled) driven oscillators, the amplitudes $\hat{V}_1, \hat{V}_2$ can experience a resonant response for a certain driving frequency. Indeed, through equations (31), (32), (34) and (35) we see that the amplitudes $\hat{V}_1, \hat{V}_2$ depend on σ. We note that the amplitudes also depend on A_{12}. Since A_{12} is an indicator for the amount of interaction, the (resonant) amplitude response of both basins is seen to depend on the amount of interaction. The goal in research sub-question 2 is to investigate the effect of this dependence on interaction. For the case of vertical basin sidewalls discussed in section 3.1, several plots were made of $\hat{V}_1, \hat{V}_2$ as functions of interaction strengths A_{12}, for two different values of forcing frequency σ: **(I)** $\sigma = 1$, i.e. close to resonance for basin 1 and **(II)** $\sigma = 1.025$, in between resonance for basin 1 and resonance for basin 2.[8] The results are explained below.

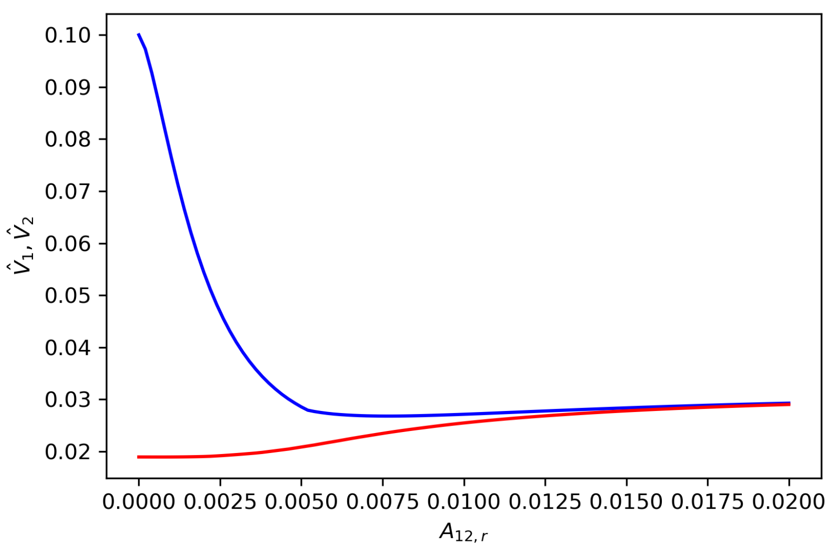

Figure 9: Response curves of $\hat{V}_1$ (blue) and $\hat{V}_2$ (red) for different values of $A_{12,r}$ (interaction strength), with parameters as in table 1 and forcing close to the Helmholtz frequency of basin 1: $\sigma = 1.00$. Note how the resonant response of basin 1 strongly diminishes as interaction increases.

<u>**Case (I):**</u> close to resonance for basin 1, $\sigma = 1$: results are visualized in Figure 9. For $A_{12,r} = 0$ the basins are not interacting, and we see the strong resonance for basin 1 which

[8] This means that forcing frequency σ lies between the resonance frequency of basin 1 and the resonance frequency of basin 2: $1 < 1.025 < 1.049 = \frac{\sigma_{H,2}}{\sigma_{H,1}}$.

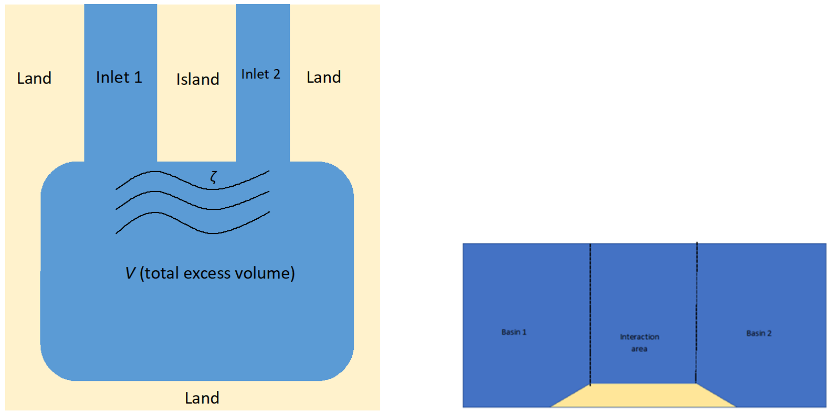

(a) (b)

Figure 10: (a) Top view of a tidal inlet system with one basin and two inlets, which the double, interacting tidal inlet system can be approximated to at large interaction, when $\zeta_1 = \zeta_2 \equiv \zeta$ and $V \equiv V_1 + V_2$. (b) Schematic side view the interaction area at large interaction values. The interaction area is now of comparable dimensions to the basins and therefore does not effectively separate the two volumes.

was already known for single tidal inlet systems. In the same manner, basin 2 is forced relatively far from resonance and its response is therefore choked at $A_{12,r} = 0$.
However, when $A_{12,r}$ increases and therefore the amount of interaction increases, it is obvious that the resonant response of basin 1 strongly diminishes. Thus, the resonant response of an interacting basin forced at its Helmholtz frequency appears to diminish as interaction increases. Note that, simultaneously, the response of basin 2 seems to become somewhat larger than before. This is speculated to be due to the notion that, when interaction increases, basin 2 absorbs some of the high water-level volume of basin 1, therefore obtaining a net increase of its own water level.
When interaction is further increased, i.e. roughly $A_{12,r} > 0.01$ in Figure 9, the interaction is large enough to facilitate that the two basins approximately behave as one large basin. This is caused by the restoring mechanism of the interaction term $\zeta_1 - \zeta_2$, which forces the free surfaces of the basins to behave identically. In Figure 9 it shows up as the blue an red graph starting to overlap for $A_{12,r} > 0.01$, indicating that the amplitudes of basin 1 and 2 are (roughly) equal.
Thus, the large interaction regime can be approximated as a tidal inlet system with a single basin and two inlets, see Figure 10a. For such a tidal inlet system, the natural frequency is a weighted root mean square of the two Helmholtz frequencies associated with the two inlets. This is shown in Appendix C. Hence, in the large interaction regime, the double tidal inlet system will effectively have a new, resultant Helmholtz frequency $\sigma_{H,eff}$, which is derived in Appendix C as $\sigma_{H,eff} = \sqrt{\frac{1+A_{2,r}\left(\frac{\sigma_{H,2}}{\sigma_{H,1}}\right)^2}{1+A_{2,r}}}$. This effective frequency, in fact, appears to explain results for case (II), discussed now.
Case (II): in between resonance for basin 1 and resonance for basin 2, $\sigma = 1.025$, see Figure 11. We see that that for large interaction, say $A_{12,r} > 0.0075$, the amplitude response of

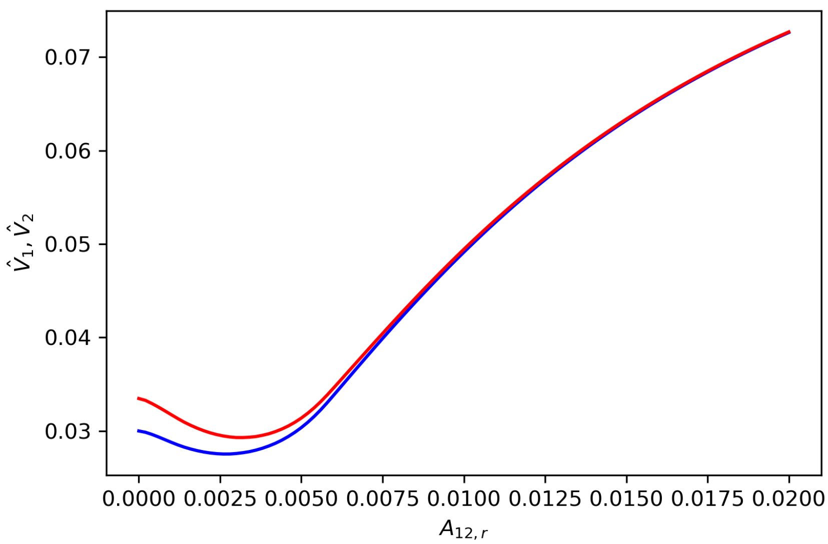

Figure 11: Response curves of of $\hat{V}_1$ (blue) and $\hat{V}_2$ (red) for different values of $A_{12,r}$ (interaction strength), with parameters as in table 1 and forcing in between resonance for basin 1 and basin 2: $\sigma = 1.025$. Note that the response of the basin increases as interaction becomes larger.

both basins actually increases for increasing interaction. This is due to the forcing frequency being close to the effective Helmholtz frequency at large interaction, as explained above. This creates a new kind of Helmholtz resonance that can only appear when the interaction is large enough such that the two basins can be approximated as one large basin.

4.2 Nonlinear model

4.2.1 Single frequency forcing

In the case of single frequency forcing near resonance, numerical integration of single tidal inlet systems with linearly sloping bottoms shows that a basin's excess volume period doubles into a period-two long-term equilibrium[9].Therefore when there is no interaction, both basins in the double tidal inlet system which is considered here will have a period two equilibrium, provided that both basins are forced near resonance. This is shown in Figure 12. The following observations are made from simulations of mono-frequency forcing:
Upon switching on interaction ($A_{12,r} > 0$), simulations indicate a distinction in response between three ranges in $A_{12,r}$-parameter space: **(A)** little interaction, **(B)** intermediate interaction and **(C)** strong interaction. For the parameter values of Table 2, little interaction corresponds to roughly $A_{12,r} < 0.001$, intermediate interaction to roughly $0.001 < A_{12,r} < 0.01$ and strong interaction to roughly $0.01 < A_{12,r}$.
Case (A): in the little interaction region of $A_{12,r}$-parameter space, the interaction term is small enough so that its perturbation of the no interaction behaviour is barely visible in

[9]For a detailed discussion, see M97.

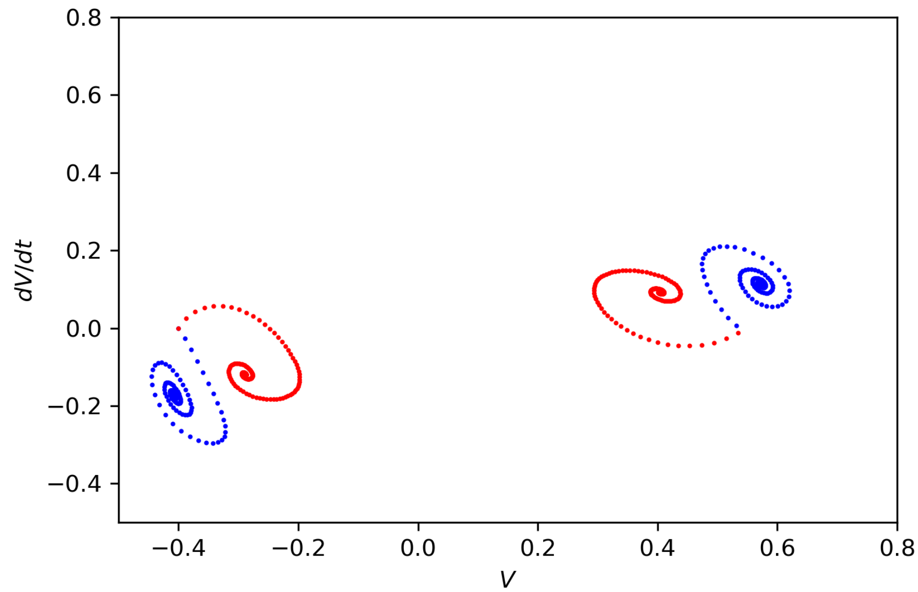

Figure 12: Poincaré map of solutions V_1 (blue) and V_2 (red) having period twice the driving period $2\pi/\sigma$. Integration started at $t = 0$, sampled period equal to the driving period $2\pi/\sigma$. Parameter values are as in table 2, where the variable parameters are $A_{12,r} = 0$, $A_{2,r} = 1.02$, $\frac{\sigma_{H,2}}{\sigma_{H,1}} = 1.016$. Initial conditions are $(V_1(0), \dot{V}_1(0), V_2(0), \dot{V}_2(0)) = (-0.4, 0, -0.4, 0)$. These parameter settings reproduce period-2 orbits similar to figure 10b of M97.

Poincaré maps and its effect is thus negligible. In general, in this region of $A_{12,r}$-parameter space, the nonlinear effects of the single tidal inlet system at no interaction are seen to retain their stability and the behaviour is qualitatively the same as for the basins when fully separated ('no interaction').

Case (B): In the intermediate interaction region of parameter space, the interaction term now seems to constitute a significant perturbation of the no interaction behaviour. In general, simulations performed show that there may exist a threshold value of $A_{12,r}$ within the intermediate interaction region for which the period two equilibria seen at no interaction lose their stability, and break down into a regular period one equilibrium. An example of this is given in Figure 13. In (a) of this figure, we see that these basins have period-2 steady states when not interacting, but in (b), the interaction is in the intermediate range and these period-2 steady states lose their stability, decaying towards a single steady state. Such a breakdown has significant implications: apparently there exist systems which exhibit nonlinear effects by themselves, but not when interacting at a certain rate. However, it seems, on the basis of performed simulations, that the window of values of $A_{12,r}$ for which this breakdown happens will be small if both basins are close to resonance. In fact, this is supported by the linear setting discussed in section 3.1. From equations (29) and (30), it follows that the amplitude of one basin is coupled to the amplitude of the other. Thus, when both basins resonate strongly, amplitudes would remain higher upon increasing interaction, and thus the effect of resonance is not strongly diminished upon increasing interaction. This could explain why the

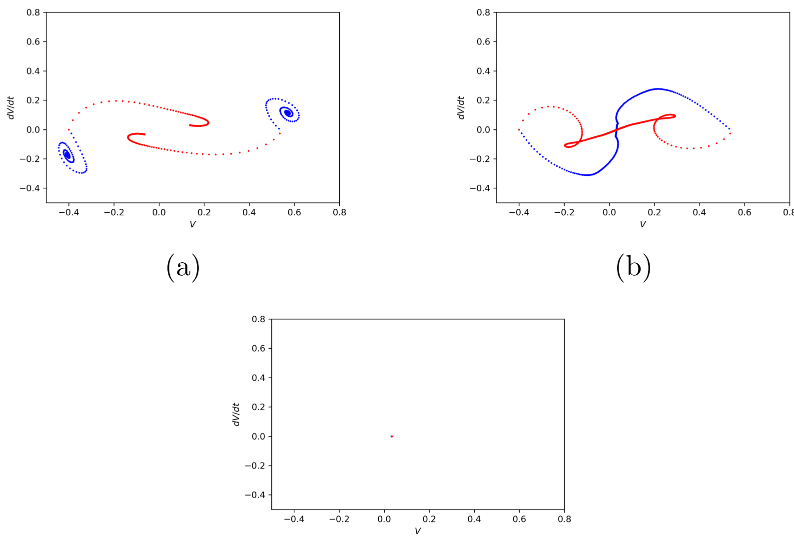

(a) (b)

(c)

Figure 13: Poincaré maps of solutions V_1 (blue) and V_2 (red) of equations (46) and (47). Parameters are as in table 2. The value of $A_{12,r}$ is different for (a),(b),(c). The other variable parameters are each time: $A_{2,r} = 1.0$, $\frac{\sigma_{H,2}}{\sigma_{H,1}} = 1.026$. Initial conditions are $(V_1(0), \dot{V}_1(0), V_2(0), \dot{V}_2(0)) = (-0.4, 0, -0.4, 0)$. (a): integration started at $t = 0$, sampling period equal to the driving period $2\pi/\sigma$; $A_{12,r} = 0$ (no interaction). Both basins have period-2 equilibria, albeit at differing amplitudes. (b): integration started at $t = 0$, sampling period equal also to the driving period. $A_{12,r} = 0.0025$ (intermediate interaction). (c) same orbit as (b) but integration started after 5000 driving periods.This makes it clear that the orbits in (b) represent a period-one steady state at late times, as only one point is visible (the blue and red points have overlapped so that only one is visible).

period-2 equilibria retain their stability for more values of $A_{12,r}$ when both basins are close to resonance.

<u>**Case (C):**</u> At large interaction, the same observation as for the linear model is made: the two basins approximately behave as one large basin. The behaviour of this one large volume can still be read off from the Poincaré maps and time series of V_1 and V_2. Now, V_1 and V_2 behave almost uniformly and both volumes give an accurate depiction of the behaviour of the total volume $V_1 + V_2$.

Also, the new effective Helmholtz frequency that arises in this approximation may serve as an an explanation for the following observation in simulations: systems which experience the aforementioned breakdown of period-two equilibria at intermediate interaction may regain period-two equilibria at large interaction. This is shown in Figure 14.

Within the approximation of considering one big basin at large interaction, the reason for the reappearance of dual equilibria in Figure 14 would be that the forcing was such that it is close to the effective Helmholtz frequency $\sigma_{H,eff}$ that is now at hand, i.e. the big basin is forced near resonance leading to two double equilibria. Actually, this reasoning further implies an important fact: the original two basins do not have to exhibit period-two equilibria at no interaction for them to do so when interacting strongly. The only requirement would be that $\sigma_{H,eff}$ is such that the forcing frequency σ is near resonance. Therefore, $\sigma_{H,1}$ and $\sigma_{H,2}$ might differ significantly from the forcing frequency, leading to no resonance and no period-two steady states at no interaction, but still produce a $\sigma_{H,eff}$ which enables resonant forcing at large interaction. This is corroborated by performed simulations. An example of this is given in Figure 15.

This is in general the only scenario from performed simulations where solutions V_1, V_2, which both show a period-one equilibrium at no interaction, can begin to show period-2 equilibria at some value of $A_{12,r}$. This is also seen for situations when only one of V_1 and V_2 shows a double period equilibrium at no interaction and the other volume tends to a period-1 equilibrium: in all simulations, at some $A_{12,r}$ the period-2 equilibrium breaks down in favour of a single equilibrium. However, as mentioned above, at large interaction period-2 equilibria might return if forcing is near the new effective Helmholtz frequency.

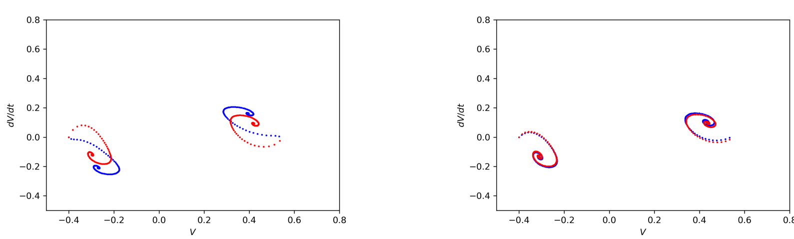

(a) (b)

Figure 14: Poincaré maps of V_1, V_2 corresponding to the same parameter settings as Figure 12, except $A_{12,r}$, which has larger values than in figure 12. Again, blue represents V_1 and red V_2. (a): $A_{12,r} = 0.01$. Evidently, period-2 equilibria have appeared again. (b) $A_{12,r} = 0.05$. In particular, the uniform behaviour of V_1 and V_2 for large interaction is clearly present in this example (the orbits almost wholly overlap).

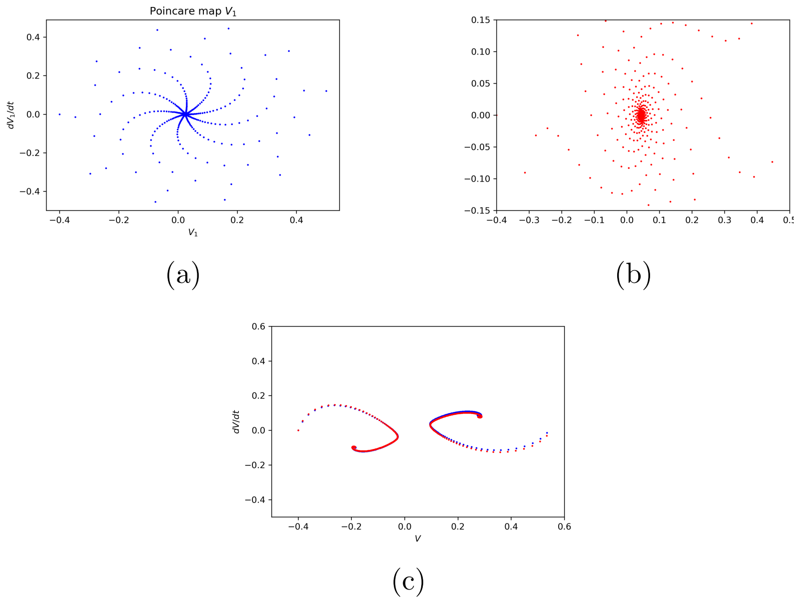

Figure 15: Poincaré maps of V_1 and V_2. Integration started at $t = 0$, sampling period equal to the driving period. The forcing frequency σ now has a different value than in Table 2: $\sigma = 2.27$. Variable parameters are $\frac{\sigma_{H,2}}{\sigma_{H,1}} = 1.24$ and $A_{2,r}$; $A_{12,r}$ is different for (a),(b) and (c). Note how σ nearly equals twice the weighted[10] root mean square of $\sigma_{H,1}$ and $\sigma_{H,2}$, being $2 \cdot \sqrt{\frac{1+1.24^2}{2}} \approx 2.253$, indicating resonant response with respect to $\sigma_{H,eff}$. (a): V_1 for $A_{12,r} = 0$ (b): V_2 for $A_{12,r} = 0$ (c): V_1 (blue) and V_2 (red) for $A_{12,r} = 0.25$.

4.2.2 Quasi-periodic forcing

In the case of quasi-periodic forcing near resonance, numerical integration of single tidal inlet systems with linearly sloping bottoms shows that a basin's excess volume can experience a chaotic response[11]. Thus, when there is no interaction, both basins in the double tidal inlet system can have such chaotic solutions, if the two forcing frequencies are near resonance for both basins. An important observation is that the window for occurrence of chaotic solutions in single tidal inlet systems seems to be very small compared to the window for period-doubling in the mono-frequency forcing case. In other words: occurrence of chaos is more sensitive to how close the forcing frequencies are to resonance. Note that, since the tides arriving in both basins have the same pair of frequencies, this effectively means that the Helmholtz frequencies of both basins have to be extremely close to each other: otherwise the forcing frequencies can impossibly be near both Helmholtz frequencies simultaneously. Because the Helmholtz frequency of a tidal inlet system depends on the geometry of the basin and inlet, this means that both basins and their inlets need to be geometrically almost identical in order to *both* exhibit chaos. An example is shown in Figure 16.

Performed simulations are different from the single frequency forcing case in two ways. Firstly, in parameter schemes where both systems are chaotic at no interaction, simulations are consistent with the statement that the basins will in fact remain chaotic for all values of interac-

[11]For a detailed discussion, see MD.

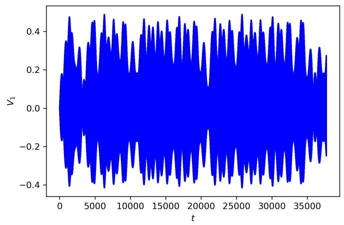

(a)

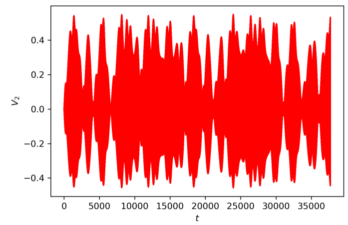

(b)

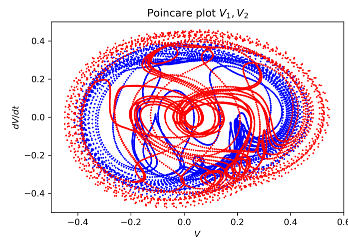

(c)

Figure 16: (a) Chaotic time evolution of V_1 at no interaction: $A_{12,r}$=0. Parameters are as in table 3; variable parameters are $A_{12,r} = 0$, $\frac{\sigma_{H,2}}{\sigma_{H,1}} = 0.995$ and $A_{2,r} = 1$. (b) Same as (a) but the plot represents V_2. (c) Poincaré map of V_1 (blue) and V_2 (red) which shows chaotic behaviour, i.e. an irregular pattern. Integration started at $t = 0$, sampling period equals the period associated with the mean of the two forcing frequencies: $\frac{\sigma_1+\sigma_2}{2}$.

tion. This contrasts to situations mentioned in the single-frequency forcing case where both basins exhibited nonlinear effects at no interaction and still lose these effects at certain interaction strengths. Secondly, when one of the volume behaves chaotically at no interaction but the other does not, the chaos of the former seems to invariably fall apart as the interaction increases. See Figure 17 for an example. In fact, this often already happens at values of $A_{12,r}$ belonging to what was described in section 4.2.1 as the 'little interaction' domain. This further attests to the more volatile nature of the chaotic solutions found in comparison to the period-2 solutions at single frequency forcing.

Interestingly, concerning large interaction, i.e. roughly $A_{12,r} > 0.01$ in the parameter settings of Table 3, results analogous to the mono-frequency case are found: basins which are unchaotic when not interacting can become chaotic at large interaction. More generally, every quasi-periodically forced double tidal inlet system with linearly sloping bottoms can become chaotic at large interaction strengths if the forcing is near resonance with respect to the new approximate effective Helmholtz frequency $\sigma_{H,eff}$. An example of unchaotic basins when not interacting that become chaotic at large interaction is given in Figure 18.

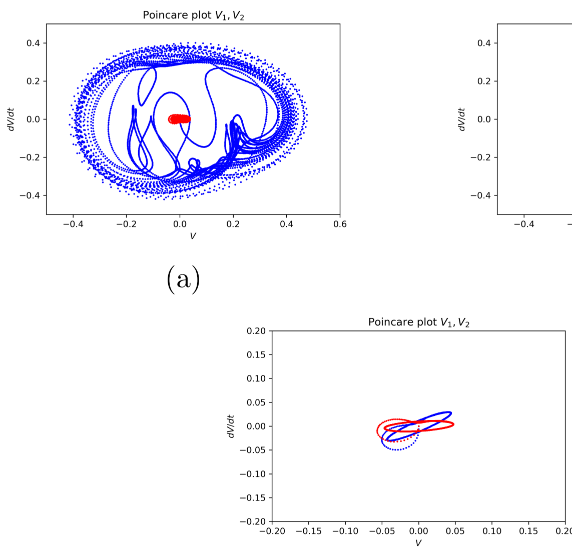

(a) (b) (c)

Figure 17: Poincaré maps of V_1 (blue) and V_2 (red). Parameters are as in table 3; variable parameters are: $\frac{\sigma_{H,2}}{\sigma_{H,1}} = 1.054$, $A_{2,r} = 1$, and $A_{12,r}$ different in (a),(b),(c). Integration started at $t = 0$, sampling period equals the period associated with the mean of the driving frequencies $\frac{\sigma_1+\sigma_2}{2}$. (a) No interaction: $A_{12,r}$=0. V_1 is chaotic, but V_2 shows a very small closed cycle, due to the quasi-period forcing, and thus does not exhibit chaos. (b) Now $A_{12,r} = 0.001$. Already, the chaotic behaviour of V_1 has lost its domain of attraction and has broken down into a closed cycle. (c) Now $A_{12,r} = 0.01$. Now V_1 is just represented by a very small closed cycle (note the V-axis length).

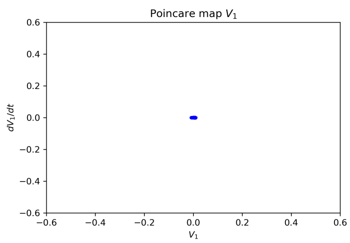

(a)

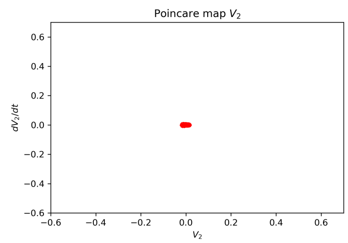

(b)

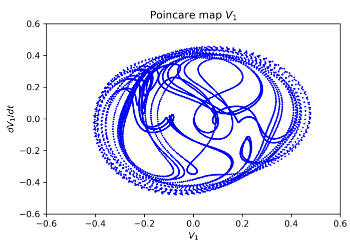

(c)

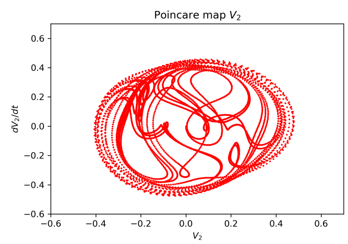

(d)

Figure 18: Poincaré maps of V_1 (blue) and V_2 (red). The parameter values of σ_1 and σ_2 are different than in table 3: $\sigma_1 = 1.13$ and $\sigma_2 = 1.14$. The parameters variable in table 3 are: $\frac{\sigma_{H,2}}{\sigma_{H,1}} = 1.24$, $A_{2,r} = 1$ and $A_{12,r}$ different for (a)+(b) and (c)+(d). Note that the $\sigma_{H,eff}$ constituted by these $\sigma_{H,1}, \sigma_{H,2}$ equals $\sqrt{\frac{1+1.24^2}{2}} \approx 1.1264$, very close to forcing. Integration started at $t = 0$, sampling period equals the period associated with the mean of the driving frequencies $\frac{\sigma_1+\sigma_2}{2}$. (a) No interaction: $A_{12,r}$=0. V_1 is not chaotic and thus looks like a closed cycle, albeit with a very small radius making it appear as a point. (b) same but for V_2 (c) Now $A_{12,r} = 0.5$: V_1 has now become chaotic. (d) same but for V_2.

5 Discussion

The articles M97 and MD established the intriguing prediction of period-doubling and chaotic phenomena in single tidal inlet systems, as first steps in theoretically explaining empirical reports on irregular tides. This thesis extends such results to two tidal inlet systems that interact with each other through a water shed. The most important results of this are summarized and further discussed below.

5.1 Linear model

From the results for the linear model (vertical sidewalls), it was found that when one of the basins was forced near-resonance, and the other was out of resonance, increasing interaction decreases the resonant response amplitude of the former basin. Thus, in general, it is found that resonance becomes less pronounced when interaction increases. A qualitative explanation for this may be that the interaction terms perturb the behaviour the individual basin would have when not interacting, thereby detuning its response.

It was also found that configurations are possible where the two basins are not near resonance when not interacting, but can experience a resonant response when interaction is sufficiently large. This is because the system now seems to behave approximately as a single basin with two inlets, for which the Helmholtz resonance frequency is a linear combination of the two Helmholtz frequencies of the individual basins. When the forcing is then close to this effective Helmholtz frequency, an amplified response is observed.

5.2 Nonlinear model

5.2.1 Single frequency forcing

As for the period-2 steady states found in M97 when the forcing is with one frequency, it is found that for all levels of interaction, double period equilibria are possible in the double tidal inlet system equivalent, though the requirements for the occurrence of double period equilibria are different for **(I)** small to intermediate interaction and **(II)** large interaction schemes.

For (I): a necessary condition for this seems to be that the forcing frequency is near resonance with respect to the Helmholtz frequencies that both tidal inlet systems have individually, so that both basins already exhibit period-2 equilibria at no interaction. If one of the basins does exhibit period-2 steady states at no interaction and the other basin has a period-1 steady state, then when interaction is switched on, the latter basin seems to always perturb the former basin out of its dual equilibrium state in the intermediate interaction range.

However, even in some scenarios where both basins exhibit period-2 equilibria at no interaction, there exists a range of interaction strengths for which the period-2 steady states lose their stability. A possible qualitative explanation of this breakdown is that the interaction is then large enough so that the volume of one basin forms a significant perturbation of the other, but that the interaction is also not large enough to force V_1 and V_2 to oscillate well in unison. This could facilitate that a smaller amplitude steady state of basin 2 perturbs the dual equilibrium of basin 1 out of its stability domain and therefore collapsing to a central equilibrium. This is consistent with the observation that the breakdown of period-2 steady states only seems to occur when there is a significant difference in early times behaviour in no interaction and small interaction ranges. Figure 13 is an example of this: at no interaction, the evolution time derivatives of the motions of V_1, V_2 are showing opposite trends in Figure 13a. On the left, $\dot{V}_1$ is negative and decreasing and $\dot{V}_2$ is positive and increasing, on the right vice versa. When interaction is switched on to a large enough degree (such as in Figure 13b), these effects will start to counteract each other resulting in the destruction of higher amplitude, double period steady states in favour of a small amplitude central steady state. This may also be indicated by the fact that the beginning of the orbits of V_1 and V_2 in Figure 13b are similar to the the ones in Figure 13a when there is still no interaction. After a certain number of cycles (i.e. a certain amount of dots in the orbits in the figure) the orbits of V_1 and V_2 seem to suddenly change behaviour with respect to no interaction situation of Figure 13a. In further research one might verify this by employing a perturbation expansion of the differential equations for volumes V_1 and V_2. This could indicate what happens to the volumes and their time derivatives during the waning of the transient effects, at the range of interaction where the aforementioned breakdown occurs. This could be compared with perturbation expansions performed in M97 for single tidal inlet systems with linearly sloping bottoms, which can be used for the no interaction scenario, where the basins behave individually as one basin.

For (II): simulations imply that a necessary condition for the occurrence of period-2 steady states of V_1 and V_2 is that the forcing is near resonance with respect to the effective Helmholtz frequency of the combined volume of V_1 and V_2. This answers the part of the research question which asks whether new nonlinear effects turn up in the double tidal inlet system model. In section 4.2.1, situations were explained where both basins' Helmholtz frequencies are not close to the forcing frequency, and therefore do not admit period-2 steady states, but their $\sigma_{H,eff}$ *is* near the forcing frequency, and therefore *does* admit period-2 steady sates. This special case of the large interaction regime can be considered as new nonlinear effects, as the period-2 equilibria were not there at no interaction, when both basins still behaved as a single tidal inlet system.

5.2.2 Quasi-periodic forcing

As for the chaotic states found in MD for a single tidal inlet system with linearly sloping sidewalls forced quasi-periodically, it is likewise found that, for all levels of interaction, chaotic states are possible in the double tidal inlet system equivalent. Again, the circumstances that allow for this to happen are different for **(I)** little to intermediate interaction and **(II)** large interaction ranges.

For (I): simulations indicate a necessary condition that parameters need to be such that the two basins already exhibit chaos when the interaction is still turned off. This implies for the forcing frequencies σ_1, σ_2 that they have to both be close to resonance. If one of the basins is not chaotic at no interaction, the chaos of the other basin is seen to readily break down when interaction is turned on, even at ranges of interaction strength which were referred to as 'small interaction' in the results section. In short, the conditions for the chaos to survive small to intermediate interaction are analogous to the conditions for period-2 steady states at single frequency, with the difference being that the chaos is more unstable and is seen to break down at, in general lower interaction strengths than the period-2 steady states.

It is also noted that no chaotic analogy was found to the situation where *both* basins exhibited period-2 steady states at no interaction and these dual equilibria still broke down at intermediate interaction. Simulations suggest that, if both basins are chaotic when there is no interaction, this chaos remains for all level of interactions.
For (II): the results were also similar to large interaction scheme in the single frequency forcing case. The necessary condition suggested by simulations is that the two forcing frequencies should be near resonance with respect to the effective Helmholtz frequency of the total volume of V_1 and V_2. Likewise do new nonlinear effects appear in situations where individual basins 1 and 2 are not chaotic when not interacting, but in fact become chaotic when interaction is added. This is possible when the Helmholtz frequencies of both basins are such that they are individually disparate from the two forcing frequencies, i.e. the forcing is not near-resonance at no interaction, but the $\sigma_{H,eff}$ they constitute at large interaction is very close to the forcing frequencies, i.e. forcing is near-resonance.

5.3 Further discussion and outlook

Still, several simplifications present in the models used in this thesis that may cast doubt on the rigorousness of the results obtained here. For example, one of the assumptions in section 2.1 was that surface elevations $\zeta_i, \zeta_{e,i}$ of tidal inlet system i were small compared to its depth scale H_i. This assumption is, however, violated in the predicted behaviour of that model: in many plots shown in the results section, excess volumes V_i regularly reach magnitudes in the range of ± 0.5, which in the scaled regime of the nonlinear model corresponds to roughly the total volume contained within basin 1. Strictly speaking, in all terms where $A_{c,i}$ appears, $i = 1, 2$, an extra term proportional to $+\zeta_i$ should be added. This leads to more complex differential equations for V_1, V_2 where some terms of the original equations now have oscillating coefficients (since $\zeta_i = \zeta_i(V_i)$), which leads to additional terms nonlinear in V_i. Therefore, one might carefully predict that chaos may still occur in this nuanced model. It should also be noted though, that the Helmholtz frequencies are also dependent on $A_{c,i}$ and the Helmholtz frequencies will therefore also evolve in an oscillatory fashion. A future study analyzing this model might also observe whether this seriously hinders the process of resonance, which is what the occurrence of nonlinear effects hinges on in this thesis.
Furthermore, the numerical analysis of the nonlinear model omitted an extra interaction term $\propto \zeta_1(V_1) - \zeta_2(V_2)$ in equations (46) and (47), aside from to the interaction term still present, which goes as $\frac{d\zeta_1}{dt} - \frac{d\zeta_2}{dt}$. It is expected that the addition of this extra term does not change the qualitative behaviour of the model much; not only because of the smallness of its prefactor compared to the prefactor of the other interaction term (already discussed in section 3.4.2, see Table 2), but it might also be argued that such a term enforces the same mechanism as the $\frac{d\zeta_1}{dt} - \frac{d\zeta_2}{dt}$-term, i.e. endeavouring to achieve that the surface elevation functions $\zeta_1(t), \zeta_2(t)$ become identically equal to each other. This would imply that the physics contained in equations (46) and (47) does not significantly change when the omitted term would be included.
Moreover, further care with omission of interaction terms should be taken when including quadratic bottom friction, which was not considered here. Both interaction terms (including

the omitted one) in equations (12) and (13) would then even be nonlinear in $(\zeta_1 - \zeta_2)$.[12] An interesting aim of a future study could be to investigate whether such a more nonlinear description of the interaction effect leads to more irregular tidal oscillations by the basins. More generally, an obvious idea for further research is to investigate whether a triple tidal inlet system with interaction between neighbours can still yield period-2 steady states and chaos. Or, more generally, whether these results remain valid for an N-tuple tidal inlet system with interaction between neighbours, where $N > 3$. This is relevant because there are systems for which reports on irregular tides were made that were multiple tidal inlet systems with water sheds, an example being the Dutch Wadden Sea, see MD.

[12] This term is itself already nonlinear in V_1, V_2 for the sloping bottom.

6 Conclusions

In this thesis, it was found that the tides generated by a coupled linear double Helmholtz oscillator, in general, oscillate with the same frequency as the forcing tide, but with a phase shift and notably a different amplitude, which depends not only on frequency, similar to a single linear driven damped oscillator, but now also on interaction strength. The tides within the two basins may still experience the Helmholtz resonance seen in single tidal inlet systems, but the when interaction is allowed, the resonant amplitude response diminishes significantly in most cases.

Results further imply that the nonlinear effects observed in M97 and MD when the basin bottoms slope linearly are also possible when the two basins are interacting through water sheds, at virtually all ranges of interaction strength. Interestingly, it was also found that some double tidal inlet systems show period-2 steady states or chaotic behaviour *only* if they interact, and not when separated. A condition for this is that the interaction zone is large enough so that the tides in the basin nearly oscillate in union.

References

[1] L. Golmen, J. Molvaer, and J. Magnusson, *Sea level oscillations with super-tidal frequency in a coastal embayment of western Norway,* Continental shelf research **14**, 1439 (1994).

[2] L. Maas and A. Doelman, *Chaotic Tides,* Journal of Physical Oceanography **32**, 870 (2002).

[3] W. Ridderinkhof, H. de Swart, M. van der Vegt, N. Alebregtse, and P. Hoekstra, *Geometry of tidal inlet systems: A key factor for the net sediment transport in tidal inlets,* Journal of Geophysical Research **10**, 6988 (2014).

[4] L. Maas, *On the nonlinear Helmholtz response of almost-enclosed tidal basins with sloping bottoms,* Journal of fluid mechanics **349**, 361 (1997).

[5] C. Mei, *The Applied Dynamics of Ocean Surface Waves* (World Scientific, 5 Toh Tuck Link, Singapore 596224, 1989), 1st ed., ISBN 9971-50-773-0.

[6] G. Carrier, R. Shaw, and M. Miyata, *The response of narrow mouthed harbors in a straight coastline to periodic incident waves,* Journal of Applied Mechanics **38**, 335 (1971).

[7] J. Taylor, *Classical Mechanics* (University Science Books, 2005), ISBN 978-1-891389-22-1.

[8] T. Open University, *Waves, Tides, and Shallow-water Processes* (Gulf Professional Publishing, 1999), 2nd ed., ISBN 978-0-08-036372-1.

[9] B. Cushman-Roisin and J.-M. Beckers, *Introduction to Geophysical Fluid Dynamics* (Academic Press, 2011), 2nd ed., ISBN 9780120887590.

[10] A. Herman, *Numerical modelling of water transport processes in partially-connected tidal basins,* Coastal Engineering **54**, 297 (2007).

A Appendix A: Derivations of equations of motion

A.1 Derivation of equations for V_1, V_2

Note that the only avenues for basins to exchange water are the basin entrance and through the interaction area (water shed). Therefore one has here

$$dV_1 = dV_{1,entr} + dV_{1,shed}, \tag{48}$$

$$dV_2 = dV_{2,entr} + dV_{2,shed}. \tag{49}$$

Note that, at the basin entrance of basin 1, the water arrives with depth-averaged velocity u_1, which is assumed to be spatially uniform. The rate of water inflow at the basin entrance is then $-u_1 A_{c,1}$, the minus sign comes from the choice that the positive x-direction is seaward. Then, in an infinitesimal time interval dt, conservation of mass implies:

$$dV_{1,entr} = -A_{c,1} u_1 dt. \tag{50}$$

Similarly, for basin 2:

$$dV_{2,entr} = -A_{c,2} u_2 dt. \tag{51}$$

For the water shed entrances, we also use conservation of mass: in time interval dt where the water is flowing in/out of basin 1 and basin 2 respectively at velocity u_{12} (positive in the direction from basin 1 to basin 2), the corresponding changes in volume are

$$dV_{1,shed} = -A_{12} u_{12} dt, \tag{52}$$

$$dV_{2,shed} = A_{12} u_{12} dt. \tag{53}$$

Substitution of the obtained expressions and division by dt yields

$$\frac{dV_1}{dt} = -A_{c,1} u_1 - A_{12} u_{12}, \tag{54}$$

$$\frac{dV_2}{dt} = -A_{c,2} u_2 + A_{12} u_{12}, \tag{55}$$

which determine V_1 and V_2 in terms of the depth-averaged flow velocities u_1, u_2 and u_{12} for which expressions are obtained in A.2.

A.2 Derivation of expressions for u_1, u_2, u_{12}

We start with the derivation of u_1; u_2 and u_{12} will follow analogously. Point of departure are the Navier-Stokes equations, which read for basin 1[13]:

$$\frac{\partial \widetilde{\mathbf{u}}_\mathbf{1}}{\partial t} + (\widetilde{\mathbf{u}}_\mathbf{1} \cdot \nabla)\widetilde{\mathbf{u}}_\mathbf{1} = \nu \nabla^2 \widetilde{\mathbf{u}}_\mathbf{1} - \frac{1}{\rho}\nabla p + \mathbf{f}_{1,body} \tag{56}$$

[13]Coriolis terms are omitted, see assumption 5) below.

where

$\widetilde{\mathbf{u}}_\mathbf{1} = (\widetilde{u}_1, \widetilde{v}_1, \widetilde{w}_1)$ is the flow velocity field in inlet 1, where the tilde indicates that the flow is not yet depth averaged;

$\mathbf{f}_{1,body} = \mathbf{g} + \mathbf{f}_{1,fric}$ is the body force exerted on a volume element;

$\mathbf{g} = (0, 0, -g)$ is gravity, where g is the acceleration of gravity;

ρ is the density of the water flowing in the system, which is assumed to be constant;

$\mathbf{f}_{1,fric}$ are frictional forces, given by $\mathbf{f}_{1,fric} = \frac{1}{\rho}\nabla \cdot \underline{\underline{\tau_1}}$;

$\underline{\underline{\tau_1}}$ is the turbulent shear stress tensor, with components $\tau_{1,ij} = -\rho \left\langle \widetilde{u}'_{1,i}\widetilde{u}'_{1,j} \right\rangle$;

$\widetilde{\mathbf{u}}'_1$ is the fluctuation of $\widetilde{\mathbf{u}}_1$, defined as $\widetilde{\mathbf{u}}'_1 = \widetilde{\mathbf{u}}_1 - \widetilde{\mathbf{u}}_{1,0}$, where $\widetilde{\mathbf{u}}_{1,0}$ is a reference value;

p is the pressure on a volume element;

ν is the kinematic viscosity.

We employ the following assumptions and boundary conditions:

1) Continuity of the pressure on the air-water boundary: pressure at free water surfaces $\zeta(x, y)$ must be equal to the athmospheric pressure and therefore (roughly) spatially constant. This means that the extra height due to variations of $\zeta(x, y)$ is negligble for the expression of the atmospheric pressure (i.e., $\frac{\partial p(\zeta(x,y))}{\partial x} = 0 = \frac{\partial p(\zeta(x,y))}{\partial y}$)

2) Continuity of the water surface at basin entrance $x = L_1$ requires that $\zeta_{s,1}(L_1^-) = \zeta_{s,1}(L_1^+) = \zeta_{e,1}$, where $x = L_1^-$ is just inside the inlet at the seaward entrance and $x = L_1^+$ is just inside the sea at the seaward entrance, subscript 's,1' denotes strait 1 (= inlet 1) and $\zeta_{e,1}$ is the surface elevation in the sea adjacent to inlet 1.

3) Continuity of water surface requires that $\zeta_{s,1}(0^+) = \zeta_{s,1}(0^-) = \zeta_1$, where $x = 0^+$ is just inside the inlet at the basin entrance and $x = 0^-$ is just inside the basin at the basin entrance and is ζ_1 is the surface elevation within basin 1.

4) The flow velocity in the inlet is assumed to be horizontally uniform and in the downstream direction, i.e. $\widetilde{\mathbf{u}}_\mathbf{1} = (\tilde{u}_1, 0, 0)^T$ and $\frac{\partial \widetilde{u}_1}{\partial x} = 0 = \frac{\partial \widetilde{u}_1}{\partial y}$ in the inlet. Similarly to the surface elevation, we assume continuity of the flow velocity $\widetilde{u}_1(0^-) = \widetilde{u}_1(0^+)$ and $\widetilde{u}_1(L_1^-) = \widetilde{u}_1(L_1^+)$. Change in flow velocity of water upon entering basin or sea thus occurs away from the boundaries of the inlet.

5) Coriolis force is neglected.

6) In the water shed, the flow velocity is assumed to vary on a slow timescale such that its time derivative is very small compared to frictional effects and pressure differences.

7) The kinematic viscosity of water is neglected: we set $\nu = 0$.

By assumption 4) the second term on the left in equation (56) is zero and by assumption 7) the first term on the right in equation (56) can be ignored. Thus, we are left with

$$\frac{\partial \widetilde{\mathbf{u}}_{\mathbf{1}}}{\partial t} = -\frac{1}{\rho}\nabla p + \mathbf{g} + \mathbf{f}_{1,fric}. \tag{57}$$

Proceeding to the equation for the z-direction:

$$0 = -g - \frac{1}{\rho}\frac{\partial p}{\partial z} \tag{58}$$

Now integrating along the vertical axis from $z' = z$ to $z' = \zeta_{s,1}$ gives:

$$p(\zeta_{s,1}(x)) - p(z) = -\rho g(\zeta_{s,1}(x) - z) \tag{59}$$

$$\Rightarrow p(x,z) = p(\zeta_{s,1}(x)) + \rho g(\zeta_{s,1}(x) - z). \tag{60}$$

Using assumption 1):

$$\frac{\partial p}{\partial x} = 0 + \rho g \frac{\partial \zeta_{s,1}}{\partial x}. \tag{61}$$

This expression for $\frac{\partial p}{\partial x}$ can be used in the x-direction equation:

$$\frac{d\widetilde{u}_1}{dt} = -g\frac{\partial \zeta_{s,1}}{\partial x} + f^x_{1,fric}. \tag{62}$$

We use the following parameterization for $f^x_{1,fric}$ (see [9], chapter 4):

$$f^x_{1,fric} = \frac{\partial}{\partial x}\left(\mathcal{A}\frac{\partial \widetilde{u}_1}{\partial x}\right) + \frac{\partial}{\partial y}\left(\mathcal{A}\frac{\partial \widetilde{u}_1}{\partial y}\right) + \frac{\partial}{\partial z}\left(\nu_\tau\frac{\partial \widetilde{u}_1}{\partial z}\right) = \frac{\partial}{\partial z}\left(\nu_\tau\frac{\partial \widetilde{u}_1}{\partial z}\right), \tag{63}$$

where $\mathcal{A}$ is a horizontal eddy viscosity and ν_τ is a vertical eddy viscosity. In particular, the two terms involving $\mathcal{A}$ vanish due to assumption 4). Substituting equation (63) into equation (62) and depth-averaging gives:

$$\begin{aligned}\frac{du_1}{dt} &= -\frac{g(\zeta_{s,1}+H_1)}{(\zeta_{s,1}+H_1)}\frac{\partial \zeta_{s,1}}{\partial x} + \frac{\nu_\tau \partial\widetilde{u}_1/\partial z\Big|_{z=-H_1}^{z=\zeta_{s,1}}}{\zeta_{s,1}+H_1} \\ &\overset{(\zeta_{s,1}\ll H_1)}{\simeq} -g\frac{\partial \zeta_{s,1}}{\partial x} + \frac{\tau_{1,\zeta_{s,1}} - \tau_{1,b}}{\rho H_1}\end{aligned} \tag{64}$$

where the flow velocity u_1 without the tilde denotes the depth-averaged flow velocity, and $\tau_{1,\zeta_{s,1}}, \tau_{1,b}$ are friction coefficients, assumed to be given by

$$\tau_{1,\zeta_{s,1}} = \tau_{wind} \equiv 0, \tag{65}$$

$$\tau_{1,b} = \rho \hat{c}_1 u_1, \tag{66}$$

where subscript 'b' denotes bottom friction.
Now integrating from $x = 0$ to $x = L_1$ and using spatial uniformity of u_1, as well as assumptions 2) and 3), yields:

$$L_1 \frac{du_1}{dt} = g(\zeta_1 - \zeta_{e,1}) - L_1 \frac{\hat{c}_1}{H_1} u_1. \tag{67}$$

This equation determines u_1 in terms of a pressure difference between the surface elevations of the basin and of the sea respectively. The equation for u_2 can be obtained simply by permutation of index 1 to index 2:

$$L_2 \frac{du_2}{dt} = g(\zeta_2 - \zeta_{e,2}) - L_2 \frac{\hat{c}_2}{H_2} u_2, \tag{68}$$

where all parameters are defined equivalently to basin 1. The expression for u_{12} is determined by a similar derivation, where the pressure difference is now provided by the difference in surface elevation on the respective sides of the water shed. By virtue of assumption 6) we additionally set $du_{12}/dt = 0$ and we obtain

$$0 = \frac{g}{L_{12}}(\zeta_1 - \zeta_2) - \frac{\hat{c}_{12}}{H_{12}} u_{12}, \tag{69}$$

which determines u_{12}. For a more detailed explanation of the dynamics in the water shed that lead to equation (69), the reader is referred to [10].

B Appendix B: Scaling

We scale as follows: $V_i = A_{0,1} H_1 V_i'$, $z = H_1 z'$, $A_i(z/H_1) = A_{0,1} A_i'(z')$, $\zeta_i = H_1 \zeta_i'$, $\zeta_{e,i} = H_1 \zeta_{e,i}'$, $u_i = U u_i'$, $u_{12} = U u_{12}'$, $t = T t'$, for $i = 1, 2$.

Substituting these new variables in equations (1)-(5), we get

$$\frac{U}{T}\frac{du_1'}{dt'} = \frac{gH_1}{L_1}(\zeta_1' - \zeta_{e,1}') - \frac{gH_1}{L_1}\left(\frac{L_1 U}{gH_1}\frac{\hat{c}_1}{H_1}\right) u_1' \tag{70}$$

$$\frac{U}{T}\frac{du_2'}{dt'} = \frac{gH_1}{L_1}\frac{L_1}{L_2}(\zeta_2' - \zeta_{e,2}') - \frac{gH_1}{L_1}\left(\frac{L_1 U}{gH_1}\frac{\hat{c}_2}{H_2}\right) u_2' \tag{71}$$

$$\begin{aligned} \frac{A_{0,1}H_1}{T}\frac{dV_1'}{dt'} =& - A_{c,1} U u_1' \\ & - A_{c,1} U \frac{A_{12}}{A_{c,1}} u_{12}' \end{aligned} \tag{72}$$

$$\begin{aligned} \frac{A_{0,1}H_1}{T}\frac{dV_2'}{dt'} =& - A_{c,1} U \frac{A_{c,2}}{A_{c,1}} u_2' \\ & + A_{c,1} U \frac{A_{12}}{A_{c,1}} u_{12}' \end{aligned} \tag{73}$$

$$0 = \frac{gH_1}{L_{12}}(\zeta_1' - \zeta_2') - \frac{gH_1}{L_{12}}\left(\frac{L_{12}}{gH_1}\frac{\hat{c}_{12}}{H_{12}}\right) u_{12}' \tag{74}$$

We then have two equations for the two unspecified velocity and time scales, respectively U and T:

$$\frac{U}{T} = \frac{gH_1}{L_1} \tag{75}$$

$$\frac{A_{0,1}H_1}{T} = A_{c,1} U \tag{76}$$

so that

$$T = \sqrt{\frac{A_{0,1}}{A_{c,1}}\frac{L_1}{g}} \equiv \frac{1}{\sigma_{H,1}} \tag{77}$$

$$U = \frac{gH_1}{L_1} T = \frac{gH_1}{L_1 \sigma_{H,1}} = H_1 \frac{A_{0,1}}{A_{c,1}} \sigma_{H,1} \tag{78}$$

where the inverse time scale $\sigma_{H,1}$ is called the Helmholtz frequency of basin 1. We thus see that the Helmholtz frequency indeed corresponds to a characteristic frequency scale.
Also, it follows from equations (77) and (78) that the following relations hold for the quantities within the parentheses in equations (70), (71):

$$\frac{L_1 U}{gH_1}\frac{\hat{c}_1}{H_1} = \frac{1}{\sigma_{H,1}}\frac{\hat{c}_1}{H_1} \tag{79}$$

$$\frac{L_1 U}{gH_1}\frac{\hat{c}_2}{H_2} = \frac{1}{\sigma_{H,1}}\frac{\hat{c}_2}{H_2} \tag{80}$$

Recognizing this, we rename $\frac{c_i}{H_i} = \frac{1}{\sigma_{H,1}}\frac{\hat{c}_i}{H_i}$ and additionally $\frac{c_{12}}{H_{12}} = \frac{L_{12}}{gH_1}\frac{\hat{c}_{12}}{H_{12}}$. Removing the primes from the nondimensional variables we arrive at the desired scaled equations:

$$\frac{du_1}{dt} = \zeta_1 - \zeta_{e,1} - \frac{c_1}{H_1}u_1, \tag{81}$$

$$\frac{du_2}{dt} = \frac{L_1}{L_2}(\zeta_2 - \zeta_{e,2}) - \frac{c_2}{H_2}u_2, \tag{82}$$

$$\frac{dV_1}{dt} = -u_1 - \frac{A_{12}}{A_{c,1}}u_{12}, \tag{83}$$

$$\frac{dV_2}{dt} = -\frac{A_{c,2}}{A_{c,1}}u_2 + \frac{A_{12}}{A_{c,1}}u_{12}, \tag{84}$$

$$0 = \zeta_1 - \zeta_2 - \frac{c_{12}}{H_{12}}u_{12}. \tag{85}$$

C Appendix C: Derivation of $\sigma_{H,eff}$

Here we provide some clarification to the given expression of the effective Helmholtz frequency at large interaction $\sigma_{H,eff}$. In the large interaction case, the double interacting tidal inlet system can be argued to behave as a single tidal inlet system with two inlets. This type of system constitutes its own Helmholtz frequency, which will be derived below.
Although in Appendix B the Helmholtz frequency for basin 1 was derived through scaling, we note that this frequency is alternatively found by calculating the prefactor of the restoring term in the (unscaled) Helmholtz oscillator equation. In a driven damped oscillator, this prefactor of the restoring term represents the square of a natural frequency (see TCM). Therefore, an (unscaled) oscillator equation for a single tidal inlet system with two inlets is required, through which the Helmholtz frequency can be read off.
The derivation is analogous to that in Appendix A, except now we consider a volume $V = V_1 + V_2$. Additionally, in the large interaction scheme, the free surfaces ζ_1, ζ_2 behave almost identically. We approximate this with $\zeta_1 = \zeta_2 \equiv \zeta$. This implies that we now have $u_{12} = 0$, which eliminates all interaction terms. Altogether, equations (54), (55), (67) and (68) are now modified to

$$\frac{dV}{dt} = \frac{dV_1}{dt} + \frac{dV_2}{dt} = -A_{c,1}u_1 - A_{c,2}u_2, \tag{86}$$

$$\frac{du_1}{dt} = \frac{g}{L_1}(\zeta - \zeta_{e,1}) - \frac{\hat{c}}{H}u_1, \tag{87}$$

$$\frac{du_2}{dt} = \frac{g}{L_2}(\zeta - \zeta_{e,2}) - \frac{\hat{c}}{H}u_2. \tag{88}$$

Friction parameters are taken to be the same in both inlets, which simplifies calculations. This is reasonable in light of performed experiments, where each time the friction parameters c_1/H_1, c_2/H_2 were taken equal to each other.
Decoupling differential equations (86)-(88) yields:

$$\frac{d^2V}{dt^2} = -\left[\frac{gA_{c,1}}{L_1} + \frac{gA_{c,2}}{L_2}\right]\zeta + \frac{gA_{c,1}}{L_1}\zeta_{e,1}(t) + \frac{gA_{c,2}}{L_2}\zeta_{e,2}(t) - \frac{\hat{c}}{H}\frac{dV}{dt}. \tag{89}$$

We further note that

$$\left[\frac{gA_{c,1}}{L_1} + \frac{gA_{c,2}}{L_2}\right] = \left[A_{0,1}\sigma_{H,1}^2 + A_{0,2}\sigma_{H,2}^2\right]; \tag{90}$$

This allows equation (89) to be written as

$$\frac{d^2V}{dt^2} = -\left[A_{0,1}\sigma_{H,1}^2 + A_{0,2}\sigma_{H,2}^2\right]\zeta + \dots\,. \tag{91}$$

The prefactor between the brackets does not have the dimensions of a squared frequency, so we clearly still have to modify the restoring term to obtain a natural frequency. Therefore, we use the sum $A_{0,1} + A_{0,2}$ as a characteristic horizontal wetted area scale for the total basin and use it in equation (91):

$$\frac{d^2V}{dt^2} = -\left[\frac{A_{0,1}\sigma_{H,1}^2 + A_{0,2}\sigma_{H,2}^2}{A_{0,1} + A_{0,2}}\right]\left[\left(A_{0,1} + A_{0,2}\right)\zeta\right] + \dots\,, \tag{92}$$

where the the prefactor between the large brackets has the dimensions of a frequency squared and the restoring term between the small brackets has the dimensions of a volume. In light of this, we define

$$\widetilde{\sigma}_{H,eff} = \sqrt{\frac{A_{0,1}\sigma_{H,1}^2 + A_{0,2}\sigma_{H,2}^2}{A_{0,1} + A_{0,2}}}, \tag{93}$$

where $\widetilde{\sigma}_{H,eff}$ denotes the unscaled version of the effective Helmholtz frequency. Upon rewriting equation (93) in terms of the scaled quantities of Appendix B, we have

$$\begin{aligned} \sigma_{H,eff} \equiv \frac{\widetilde{\sigma}_{H,eff}}{\sigma_{H,1}} &= \frac{1}{\sigma_{H,1}}\sqrt{\frac{1/A_{0,1}}{1/A_{0,1}}}\sqrt{\frac{A_{0,1}\sigma_{H,1}^2 + A_{0,2}\sigma_{H,2}^2}{A_{0,1} + A_{0,2}}} \\ &\overset{(A_{2,r}=A_{0,2}/A_{0,1})}{\Rightarrow} \sigma_{H,eff} = \sqrt{\frac{1 + A_{2,r}\left(\frac{\sigma_{H,2}}{\sigma_{H,1}}\right)^2}{1 + A_{2,r}}}. \end{aligned} \tag{94}$$

We thus see that $\sigma_{H,eff}$ is given by a 'weighted quadratic mean' of the Helmholtz frequencies of the individual basins.